

Article

Study of Decay Mechanisms and Rules of Recycled Asphalt Pavement via a Full-Scale Experiment

Quanping Xia ^{1,2}, Jiangping Gao ¹, Qigong Zhang ³, Bin Xu ⁴, Qiang Sun ^{5,*}, Ke Sun ⁶ and Zhaodi Yuan ⁵ 

¹ School of Highway, Chang'an University, Xi'an 710061, China; xiaroad@163.com (Q.X.); huangjr0124@163.com (J.G.)

² Shandong Transportation Service Center, Jinan 250001, China

³ Dongying City Highway Development Center, Dongying 257091, China; 13589986189@163.com

⁴ Shandong High-Speed Group Co., Ltd., Jinan 250098, China; cyc1070@163.com

⁵ Shandong Transportation Institute, Jinan 250102, China; yuanzhaodi365@163.com

⁶ Jinan International Airport Co., Ltd., Jinan 250107, China; echo_sk@hotmail.com

* Correspondence: sunqiang@sdjtky.cn

Abstract: Under the influence of long-term vehicle loads and large attenuation degrees, asphalt pavement performance gradually decreases, which leads to failure in fulfilling the appropriate requirements and, in turn, may affect driving safety. The purpose of this paper was to study the attenuation mechanism and rule of styrene-butadiene-styrene (SBS)-modified recycled asphalt pavement, so as to determine the applicable position and rational utilization of recycled asphalt mixture. To achieve this goal, two structures were designed, and full-scale experiments were carried out. The performance of the field test road based on accelerated loading testing (ALT) was analyzed through field monitoring data. The fatigue characteristics of stone matrix asphalt-13 (SMA-13) and asphalt concrete-20 (AC-20) mixtures before and after accelerated loading were studied via the trabecular bending fatigue test and dynamic modulus test. The microscopic components in the asphalt mixtures were determined via thin-layer chromatography on chromarods with flame ionization detection (TLC-FID). The results showed that the fatigue properties of recycled asphalt mixture can meet the requirements of ordinary asphalt mixtures and meet the technical standards of asphalt pavement design. With the increase in loading times, the British pendulum number (BPN) value of the two structures tended to be stable, and the BPN of Plan 2 was six less than that of Plan 1. Under the same test conditions, the fatigue life sequence of the recycled asphalt mixture under different loading frequencies was 20 Hz > 10 Hz > 5 Hz. The contents of four components in the reclaimed asphalt mixture were similar to those in the ordinary asphalt mixture. The light component of the reclaimed asphalt mixture of SMA-13 was reduced by 11.69%, and the light component of the ordinary asphalt mixture of SMA-13 was reduced by 15.29% through the full-scale test. In summary, recycled asphalt mixture should not be applied to the upper layer of pavement but can be rationalized in the middle layer and the bottom layer of pavement.

Keywords: recycled asphalt pavement; decay mechanism; fatigue equations; full-scale experiment; rod-shaped thin-layer chromatography test



Citation: Xia, Q.; Gao, J.; Zhang, Q.; Xu, B.; Sun, Q.; Sun, K.; Yuan, Z. Study of Decay Mechanisms and Rules of Recycled Asphalt Pavement via a Full-Scale Experiment. *Coatings* **2023**, *13*, 1955. <https://doi.org/10.3390/coatings13111955>

Academic Editor: Andrea Simone

Received: 19 September 2023

Revised: 3 November 2023

Accepted: 7 November 2023

Published: 16 November 2023



Copyright: © 2023 by the authors. Licensee MDPI, Basel, Switzerland. This article is an open access article distributed under the terms and conditions of the Creative Commons Attribution (CC BY) license (<https://creativecommons.org/licenses/by/4.0/>).

1. Introduction

In recent years, the number of roads has soared, playing an important role in global economic development [1–5]. Most of the roads built in the early stages of development have gradually entered the maintenance period. Asphalt pavement recycling technology conforms to the concept of sustainable development and green highway construction and is gradually being popularized and applied [6–9].

At present, the research on recycled asphalt mixture mainly focuses on different production processes and recycled asphalt pavement (RAP) content, and the results have shown that recycled asphalt mixture has better pavement performance [10–17]. However,

since the damage of asphalt pavement is mainly fatigue damage [18,19], many road engineers are skeptical about the long-life performance of asphalt pavement regeneration technology; therefore, it is particularly important to assess the long-life performance of recycled asphalt pavement [20].

Under long-term vehicle loads and large attenuation degrees, pavement performance of asphalt pavement will be reduced, affecting driving safety. Scholars have often used full-scale experiments to simulate the long-term driving effect on asphalt pavement and study the long-life performance of asphalt mixtures [21–23]. Load, temperature, water and asphalt mixture types all lead to fatigue failure of pavement to varying degrees [24–27]. Wu et al. found that the amount of rut deformation in the pavement increased year by year during a five-year observation period, and the driving comfort was seriously affected [28]. Xu et al. analyzed the relationship between the skid resistance index and the number of accelerated loading cycles and established a logarithmic model to characterize the long-term skid resistance of asphalt pavement [29]. Park conducted a dynamic load simulation on the pavement surface profile, vehicle speed, and vehicle suspension, and their study showed that the fatigue life of the 12.5 mm + PG64-22 asphalt mixture decreased more than that of the 12.5 mm + PG58-22 asphalt mixture [30]. Although there have been a large number of experiments conducted to analyze the recycled asphalt mixture, most of the relevant research has focused on optimizing a specific aspect of its performance, such as its rut deformation or skid resistance. However, previous studies on the fatigue properties of different types of recycled asphalt mixtures under accelerated loads have not been comprehensive enough. The causes of aging of recycled asphalt mixtures have not been analyzed from the microscopic point of view, and no specific suggestions on their application location have been provided.

In this study, the variation law of pavement service performance was established through full-scale experiments and field monitoring. Trabecular bending fatigue tests of pavement structure specimens after accelerated loading were carried out and compared with those without loading, and fatigue equations for the recycled asphalt mixture under different load frequencies were obtained. Rod-shaped thin-layer chromatography (TLC-FID) was used to detect the microscopic components of the recycled asphalt mixtures of SMA-13 and AC-20 after accelerated loading, and the differences in the saturates, aromatics, resins, and asphaltenes under different conditions were analyzed.

2. Experimental Background

2.1. Sample Preparation

2.1.1. Test Road Surface Material

The test road surface materials are shown in Table 1.

Table 1. Test road material classification.

Serial Number		Material Classification
I	I-1	SMA-13 ordinary asphalt mixture
	I-2	SMA-13 ordinary asphalt mixture (after accelerated loading)
II	II-1	SMA-13 recycled asphalt mixture
	II-2	SMA-13 recycled asphalt mixture (after accelerated loading)
III	III-1	AC-20 recycled asphalt mixture
	III-2	AC-20 recycled asphalt mixture (after accelerated loading)

1. SMA-13 ordinary asphalt mixture.

According to the screening results of each hot silo, after calculating and adjusting the grading of the mineral mixture close to the target mix ratio, the weight ratio of each hot silo was determined to be the following: the 3# hot silo (10–15 mm) accounted for 43.0%, the 2# hot silo (5–10 mm) accounted for 34.0%, the 1# hot silo (0–3 mm) accounted for 13%,

and the mineral powder accounted for 10%. The synthetic grading curve is displayed in Figure 1. The optimal design oil–stone ratio was determined to be 6.30%.

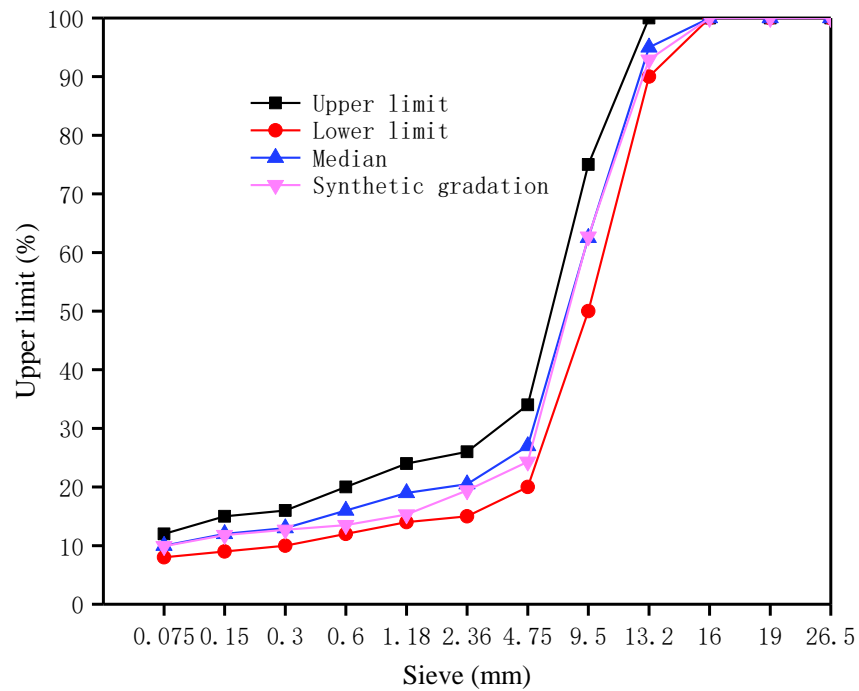


Figure 1. The synthetic grading curve of the SMA-13 ordinary asphalt mixture.

2. SMA-13 recycled asphalt mixture.

According to the screening results of each hot silo, after calculating and adjusting the grading of the mineral mixture close to the target mix ratio, the weight ratio of each hot silo was determined to be as follows: the 1#RAP silo (coarse material) accounted for 9%, the 2#RAP silo (fine material) accounted for 11%, the 3# hot silo (10–15 mm) accounted for 31.0%, the 2# hot silo (5–10 mm) accounted for 32.0%, the 1# hot silo (0–3 mm) accounted for 8.5%, and the mineral powder accounted for 8.5%. The synthetic grading curve is shown in Figure 2. The optimal design oil–stone ratio was determined to be 6.10%.

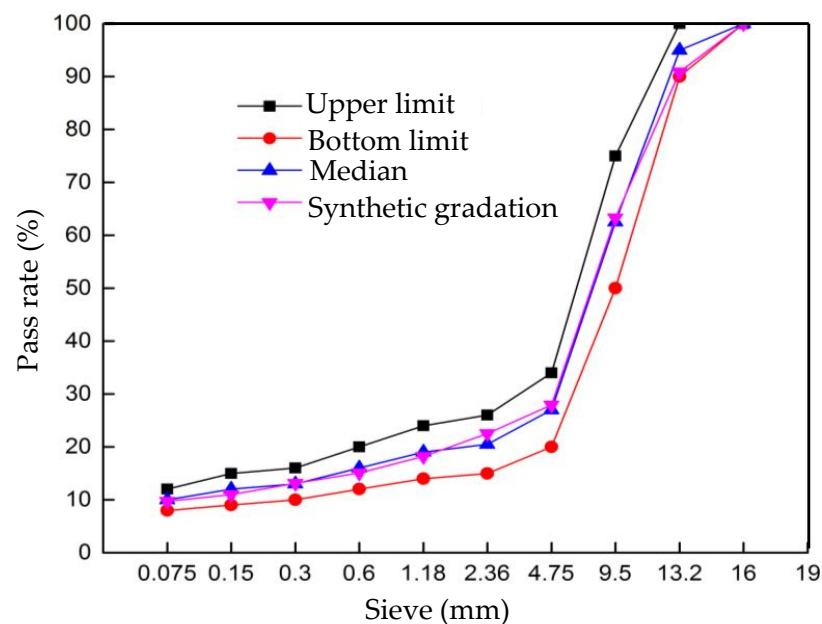


Figure 2. The synthetic grading curve of the SMA-13 recycled asphalt mixture.

3. AC-20 recycled asphalt mixture.

According to the screening results of each hot silo, after calculating and adjusting the grading of the mineral mixture close to the target mix ratio, the weight ratio of each hot silo was determined to be as follows: the 4# hot silo (19–32 mm) accounted for 18%, the 3# hot silo (11–19 mm) accounted for 21%, the 2# hot silo (6–11 mm) accounted for 8%, the 1# hot silo (0–3 mm) accounted for 10%, the 1#RAP silo accounted for 40%, and the mineral powder accounted for 3%. The regeneration agent was 5% of the old asphalt. The synthetic grade curve is displayed in Figure 3. The optimal oil–stone ratios were determined to be 4.31% and 4.50%, respectively.

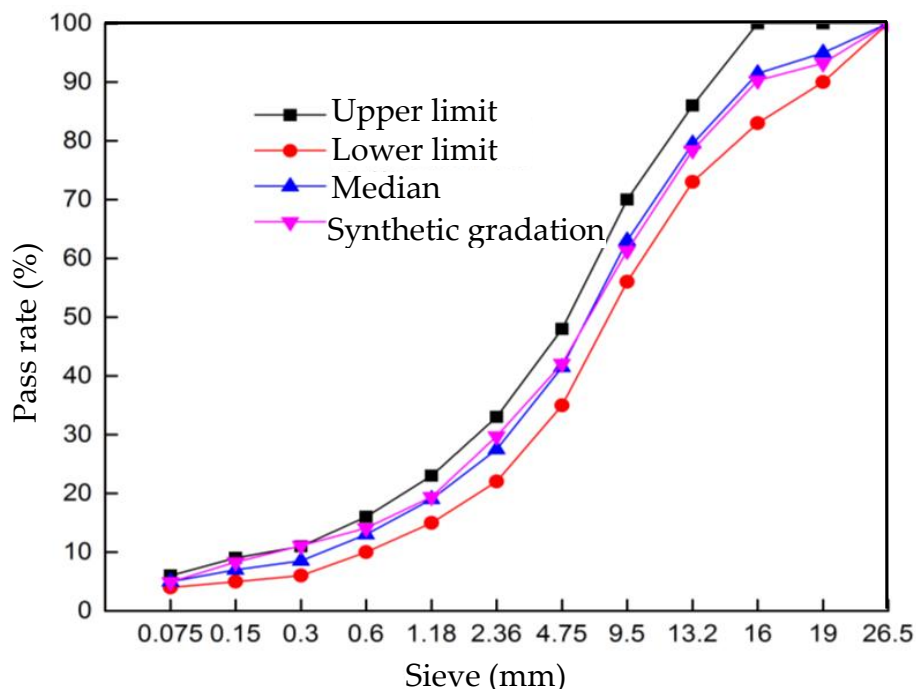


Figure 3. The synthetic grading curve of the AC-20 recycled asphalt mixture.

2.1.2. Performance Evaluation

1. Water stability.

According to the design grading and the optimal oil–stone ratios of the SMA-13 and AC-20 recycled asphalt mixtures given in Section 2.1, four groups of Marshall test pieces were made, and a Marshall test, a 48 h immersion Marshall test, and a freeze–thaw splitting test were conducted (50 compaction times of specimens) [31,32]. The water stability of the asphalt mixture was verified. The residual stability of SMA-13 was 91.8%, and its residual strength ratio was 85.5%. The residual stability and the residual strength ratio of AC-20 were 83.7% and 98.9%, respectively, both of which met the requirements of the specification.

2. Rutting resistance.

Rutting tests were carried out on the asphalt mixtures with the design grades of SMA-13 and AC-20 and the optimum oil-to-stone ratio at the temperature of 60 °C and wheel pressure of 0.7 MPa. The specimen size was 30 cm × 30 cm × 5 cm. The test results are shown in Table 2. SMA-13 met the design requirement of not less than 3000 times/mm, while AC-20 met the design requirement of not less than 1000 times/mm.

Table 2. Rutting test results.

Type of Asphalt Mixture	Oil–Stone Ratio	Dynamic Stability (times/mm)
SMA-13 recycled asphalt mixture	6.10	>6000
AC-20 recycled asphalt mixture	4.50	2896

3. Low-temperature crack resistance.

The design grading of the SMA-13 recycled asphalt mixture and the AC-20 recycled asphalt mixture and the optimal amount of asphalt were determined, and the low-temperature bending test was carried out on them. The specimens were prismatic trabeculars with a length of $250 \text{ mm} \pm 2.0 \text{ mm}$, a width of $30 \text{ mm} \pm 2.0 \text{ mm}$, and a height of $35 \text{ mm} \pm 2.0 \text{ mm}$ cut using the rutting plate after wheel grinding, with a span of $200 \text{ mm} \pm 0.5 \text{ mm}$.

The low-temperature bending test of the asphalt mixture was carried out under the conditions of a $-10 \text{ }^\circ\text{C}$ temperature and a 50 mm/min loading rate to measure the failure strength, failure strain, and failure stiffness modulus and to comprehensively evaluate the low-temperature crack resistance of the asphalt mixture [33,34]. The low-temperature bending test data for the SMA-13 recycled asphalt mixture are shown in Table 3, and the low-temperature bending test data for the AC-20 recycled asphalt mixture are shown in Table 4.

Table 3. The low-temperature bending test data for the SMA-13 recycled asphalt mixture.

Index Number	The Flexural Tensile Strength of the Specimen under Failure, R_B (MPa)	Maximum Flexural Tensile Strain at Failure of Specimen, $\varepsilon_B \times (10^{-6})$	The Bending Stiffness Modulus of the Specimen under Failure, S_B (MPa)
1	8.38	3371	2485
2	8.86	3898	2274
3	12.88	4387	2936
4	8.67	4222	2054
5	10.02	4064	2464
6	10.98	5232	2099
7	10.68	5218	2048
8	9.84	4806	2048
Average value	10.04	4399.7	2301
Technical requirement	-	≥ 2500	-

Table 4. The low-temperature bending test data for the AC-20 recycled asphalt mixture.

Index Number	The Flexural Tensile Strength of the Specimen under Failure, R_B (MPa)	Maximum Flexural Tensile Strain at Failure of Specimen, $\varepsilon_B \times (10^{-6})$	The Bending Stiffness Modulus of the Specimen under Failure, S_B (MPa)
1	11.28	3207	3517
2	9.70	3683	2635
3	9.32	3923	2376
4	10.11	3502	2886
5	11.16	4748	2350
6	10.77	3417	3152
7	9.24	3293	2804
8	11.30	2923	3869
Average value	10.36	3587	2949
Technical requirement	-	≥ 2500	-

2.2. Test Methods and Scheme

2.2.1. Full-Scale Experiment

The test road was divided into two different pavement structures: the base cement stabilized gravel, with a thickness of 360 mm , and the bottom layer is the AC-20 recycled asphalt mixture, with a thickness of 60 mm . The top layer of the SMA-13 recycled asphalt mixture and the SMA-13 ordinary asphalt mixture was 40 mm thick. The site layout of the full-scale experiment is shown in Figure 4. In order to carry out an effective comparison test, 30 m (K205 + 820–K205 + 850) of the 150 m test road was of the SMA-13 ordinary asphalt mixture, and the remaining 120 m (K205 + 700–K205 + 820) was of the SMA-13 recycled asphalt mixture, as shown in Table 5 and Figure 5.



Figure 4. Site layout of the full-scale experiment.

Table 5. Test section pavement structure combination.

Plan	The Upper Layer (Thickness of 40 mm)	The Bottom Layer (Thickness of 60 mm)
Plan 1	SMA-13 ordinary asphalt mixture	AC-20 recycled asphalt mixture; RAP content is 40%
Plan 2	SMA-13 recycled asphalt mixture; RAP content is 20%	AC-20 recycled asphalt mixture; RAP content is 40%

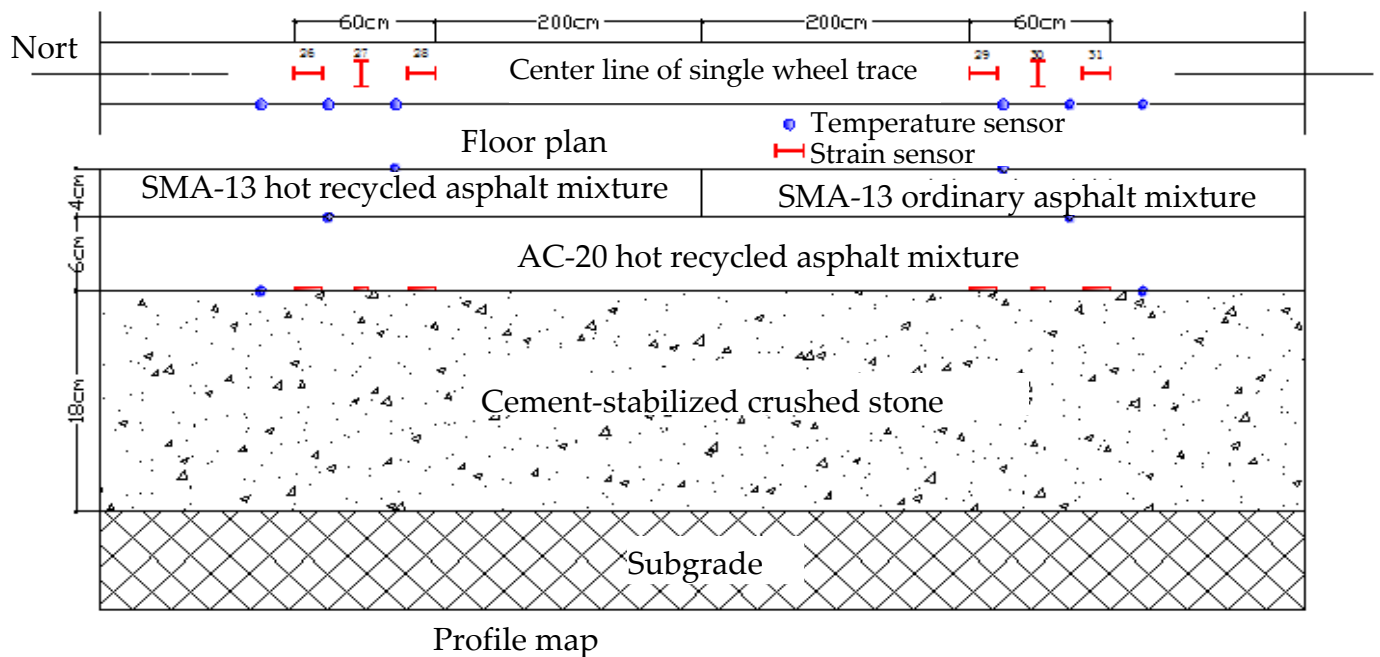


Figure 5. Test pavement structure drawing.

ALT large acceleration loading equipment was used. The maximum external dimensions, length × width × height, were 26,342 mm × 4220 mm × 7934 mm. The maximum gradient was 6%, the maximum transverse was 3%, the loading length was 10 m, the running speed was 24.6 km/h, and the shaft load was 150 kN.

2.2.2. Field Monitoring Method

A resistance strain gauge in the shape of an “I” was buried in the test section. The field layout diagram of the sensor in the field test road and the location and wiring of the

strain gauge are shown in Figure 6. The strain gauge was installed using the method of core hole superposition excavation. The depth was about 60 mm. At the edge of the core hole, the slit length was about 200 mm, made using a slit cutter.



Figure 6. Sensor mounting position. (a) Field layout of sensors on the field test road. (b) Location and wiring of the strain gauge.

The more commonly used embedded thermocouple temperature sensor was adopted, which has a large measuring range and high accuracy up to 0.002 °C. The temperature sensors P1 and P2 were embedded, and P3 was excavated. The difference between the measured data from the three temperature sensors was within 0.1 °C, and the average value of the three data points was taken as the final measurement. In order to facilitate data reading, the strip and display were transformed into the plug-and-read display, as shown in the figure, and the temperature was recorded once every hour. In the field test section, the DI-510-32 data acquisition system (see Figure 7) could be used to extract sample dynamic data from the system.

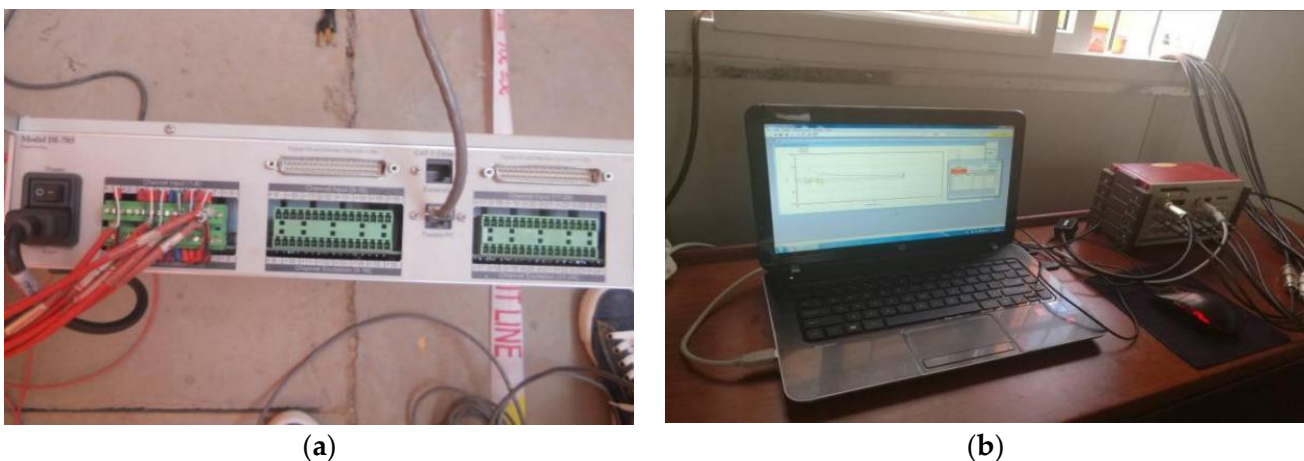


Figure 7. Data acquisition system. (a) Strain data acquisition. (b) Sensor indoor detection.

1. Pavement temperature monitoring.

In order to continuously and automatically detect the temperature field of the accelerated loading site, an automatic temperature field acquisition system was added, as shown in Figure 8. The locations of the temperature field data collection were set at 1/2 thickness of the water stabilization base, and 1/2 thickness of the upper layer and bottom layer, the road surface, and in the air. According to field testing experience, the collection interval was set to 30 min.

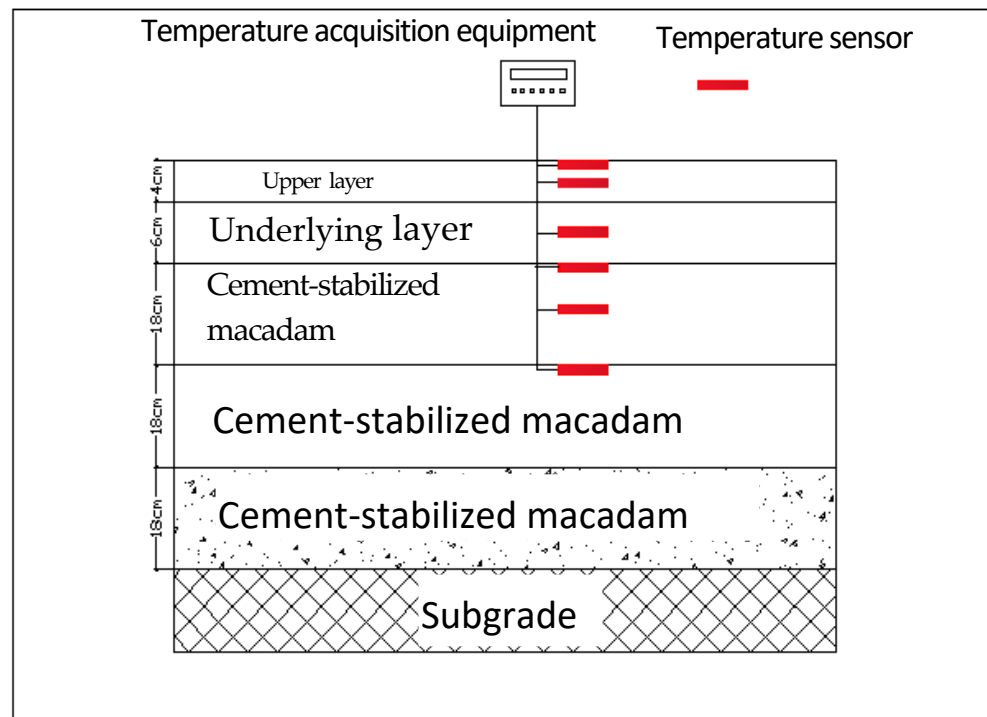


Figure 8. Layout diagram of an automatic pavement temperature field acquisition system.

2. Skid resistance monitoring.

In the full-scale experiment, the pendulum tribometer was used to monitor the BPN, and the data from the test road were collected every 5000 loading times. During the test, the friction coefficient was detected at a fixed point, and 4 detection points (a total of 8 measurement points) were set for the 2 wheel tracks. Figure 9 shows the layout of the fixed monitoring points.

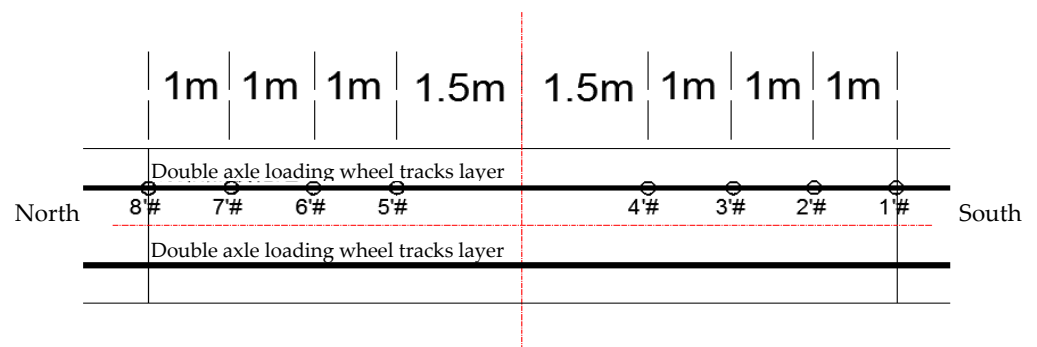


Figure 9. Schematic diagram of the fixed monitoring points.

3. Rut monitoring.

This full-scale experiment road adopted a 3 m straightedge to collect rutting data every 5000 loading times. According to previous experience, rutting appears more obvious under a high-temperature environment and heavy load, and it serves as the main control index of pavement fatigue failure.

4. Monitoring of tensile and compressive strain in the asphalt layer bottom.

The tensile and compressive strain data from the bottom layer were collected every 5000 loading times in this loading acceleration test. According to previous experimental observations, the whole-day temperature difference in coastal cities is large. As such, the bottom strain was greatly affected by the bottom temperature of the pavement. Therefore,

the strain data were collected once an hour, and the dynamic change in strain value under loading times at the same temperature was compared.

2.2.3. Trabecular Bending Fatigue Test

After the completion of the field ALT full-scale experiment, the field test road was sampled. The representativeness of the field core sample was strong, and it was of great significance to test and analyze the asphalt mixture fatigue performance of the field core sample. The specimen size was 500 mm × 400 mm × 100 mm. The specimens are shown in Figure 10.

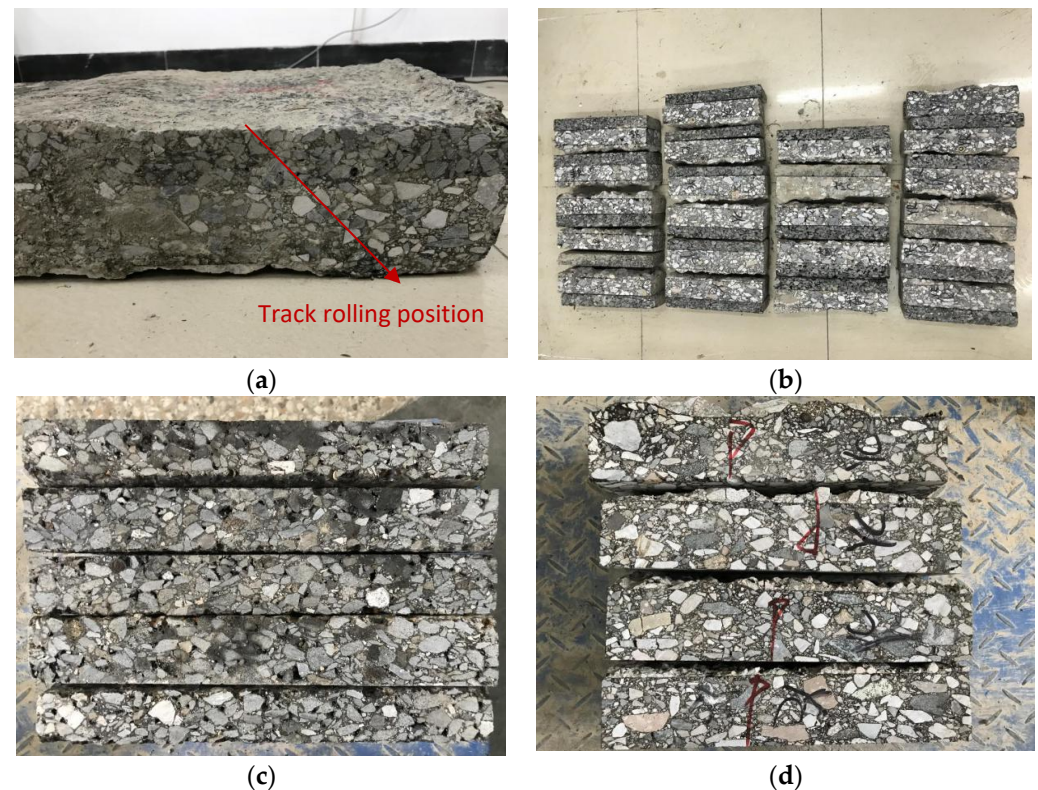


Figure 10. The specimen diagram. (a) Field sample diagram. (b) Field rectangular sample. (c) Trabecular cutting specimen of SMA-13. (d) Trabecular cutting specimen of AC-20.

Under room temperature, an asphalt mixture exhibits significant viscoelastic properties [9]. With the increase in the number of loads, the specimen's flexural residual deformation gradually increases, the stiffness (or modulus) of the material gradually decreases, micro-cracks continuously develop, and, finally, there is a complete fracture. As this expression is simple and clear, and the test data are stable, the complete fracture of the specimen is usually taken as the fatigue failure standard under the control of stress.

A trabecular bending fatigue test, using the MTS-810 material testing machine, was carried out according to the specification requirements and test scheme design. The trabecular bending fatigue test is displayed in Figure 11. The specific test steps are as follows:

- (1) The standard specimen is stored in a YDDL 40-440 digital display high- and low-temperature refrigerator (15 °C) for two hours.
- (2) The MTS environment chamber regulates the constant temperature (15 °C).
- (3) The specimen is placed on the mold.
- (4) The initial contact load is set via MTS. The specimen is in contact with the load device.
- (5) The load is applied according to the design requirements.
- (6) The test data are collected according to the design requirements.

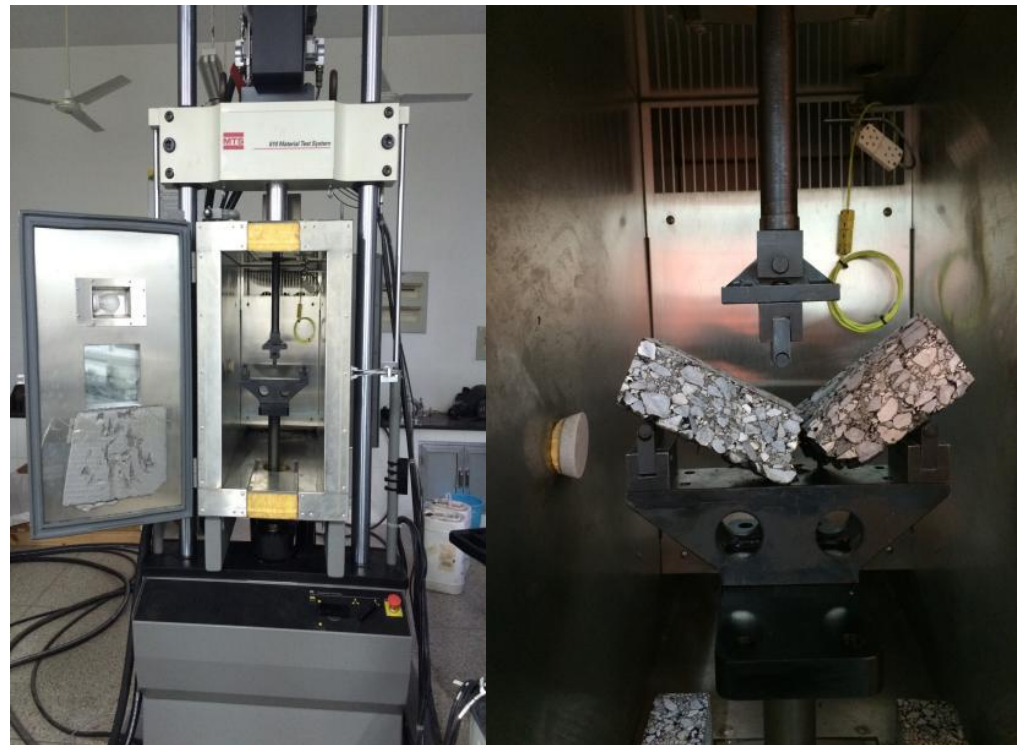


Figure 11. MTS environmental chamber, loading die, and MTS load test.

This test adopts the stress control loading mode and three-point loading [35]. The loading waveform and frequencies in this paper were continuous semi-positive vector loads of 5 Hz, 10 Hz, and 20 Hz, and the stress ratios were 0.2, 0.3, 0.4, 0.5, and 0.6. The test temperature was 15 °C.

2.2.4. Dynamic Modulus Test

For the core samples taken on site, a core sample with a diameter of $\phi 100$ mm was drilled using a core machine; then, after cutting and polishing, the height of the specimen met the test requirements, as shown in Figure 12a.

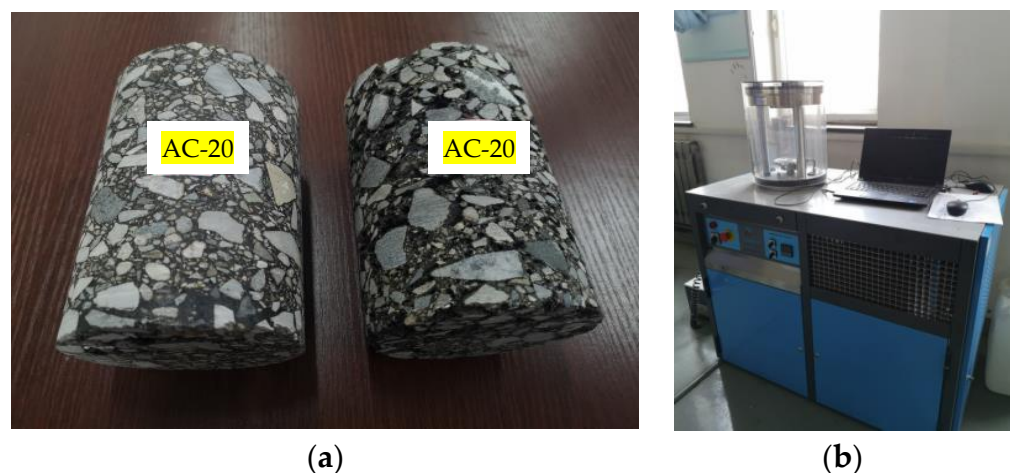


Figure 12. Data acquisition system. (a) Specimen. (b) AMPT dynamic modulus testing machine.

The dynamic modulus test was carried out according to the test methods of “Standard Method of Test for Determining Dynamic Modulus of Hot Mix Asphalt (HMA)” AASHTO TP62 and “Standard Test Methods of Bitumen and Bituminous Mixtures for Highway Engineering” JTG E20-2011 (T0738-2011) [36,37]. The instrument used in the dynamic

compressive resilience modulus test system was the asphalt mixture simple performance test (AMPT). The AMPT dynamic modulus testing machine is shown in Figure 12b. The four temperatures of 6 °C, 21.1 °C, 37 °C, and 54 °C were adopted in the test process, and the following loading frequencies of 25 Hz, 20 Hz, 10 Hz, 5 Hz, 2 Hz, 1 Hz, 0.5 Hz, 0.2 Hz, and 0.1 Hz were adopted at each test temperature. This test adopted the constant strain control mode, and the sinusoidal load was applied to the specimen. The control range of strain varied from 75 μm to 125 μm centimeters.

2.2.5. Rod-Shaped Thin-Layer Chromatography Test

This experiment employed TLC-FID to test the microscopic components of the recycled material, which involved the analysis of the saturate, aromatic, resin, and asphaltene components' differences under different conditions [38]. The rod-shaped thin-layer chromatography instrument in shown in Figure 13.

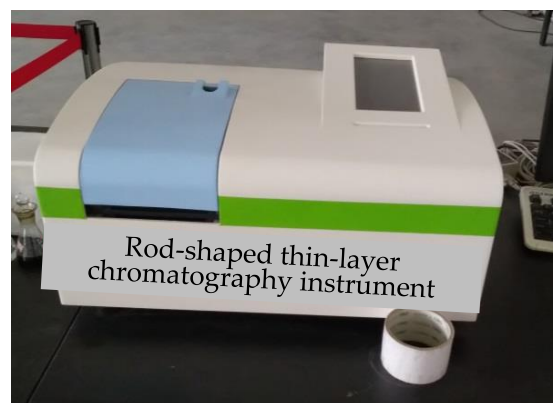


Figure 13. Rod-shaped thin-layer chromatography instrument.

The test process of the TLC-FID analysis of the four components of asphalt is shown in Figure 14, and the test conditions are shown in Table 6.

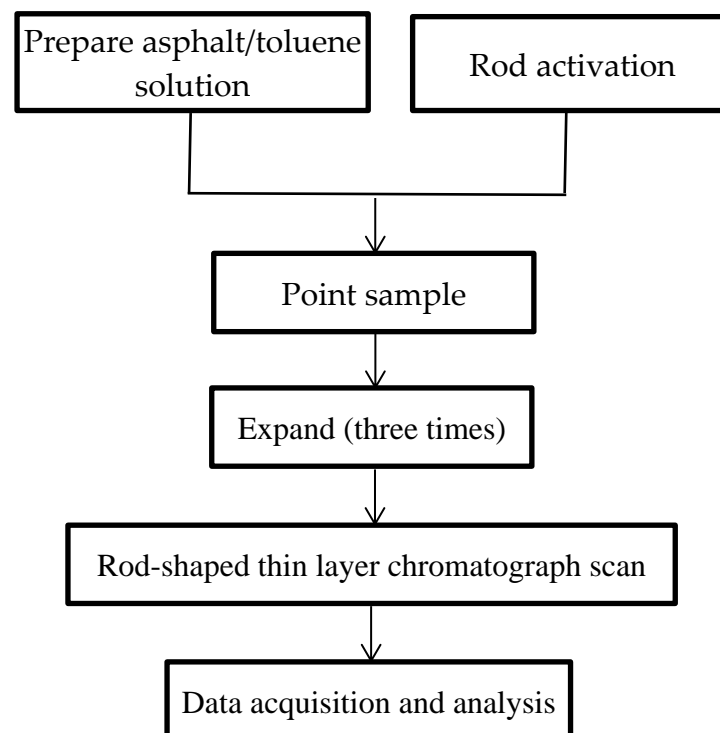


Figure 14. The test process of TLC-FID analysis of four components of asphalt.

Table 6. Test conditions.

Test Condition	Parameter
Air flow	2.0 L/min
Hydrogen flow rate	160 mL/min
Test rate	30 s/scan
Activation rate	50 s/scan
Rod load	100–150 μg
Sampling quantity	1 μL

3. Results and Discussion

3.1. Study on the Service Performance of a Field Test Road Based on ALT

3.1.1. Temperature Variation in Asphalt Pavement

The relation curve between pavement loading times and temperature is shown in Figure 15. Due to the long period of the full-scale experiment, the temperature during the test changed with the ambient temperature. It can be seen that the temperature measured in Figure 15 is divided into two stages. In the first stage, the average temperature of the upper layer of the pavement was 57.9 °C, the average temperature of the bottom layer of the pavement was 36.2 °C, and the total number of loading times was 120,000. In the second stage, the average temperature of the upper layer of the pavement was 36.8 °C, the average temperature of the bottom layer of the pavement was 26.3 °C, and the total number of loading times was 180,000. With the increase in loading times, the temperature of the pavement decreased. The temperature of the upper layer of the pavement was 25% lower than that of the bottom layer of the pavement, indicating that the upper layer of the pavement was more affected by ambient temperature and loading.

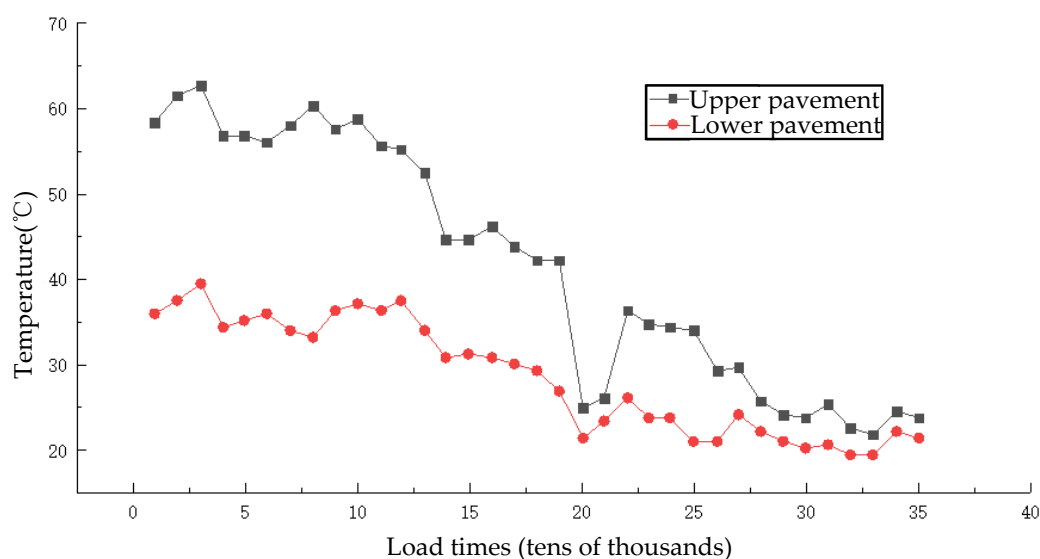


Figure 15. Temperature change curve during loading times.

3.1.2. Skid Resistance Variation in Asphalt Pavement

The results of a systematic analysis of the change results of the friction coefficient after different rolling times are shown in Figure 16. After loading the two pavement structures, their swing values rapidly decreased in the early stage, but with the gradual increase in loading times, the two pavement structures had different changes. When the loading times of Plan 1 reached 100,000, the BPN reached 44 and then slowly decreased. When the loading times of Plan 2 reached 140,000, the BPN dropped to 38, six less than that of Plan 1. Under the same external conditions, the BPN of Plan 1 was larger.

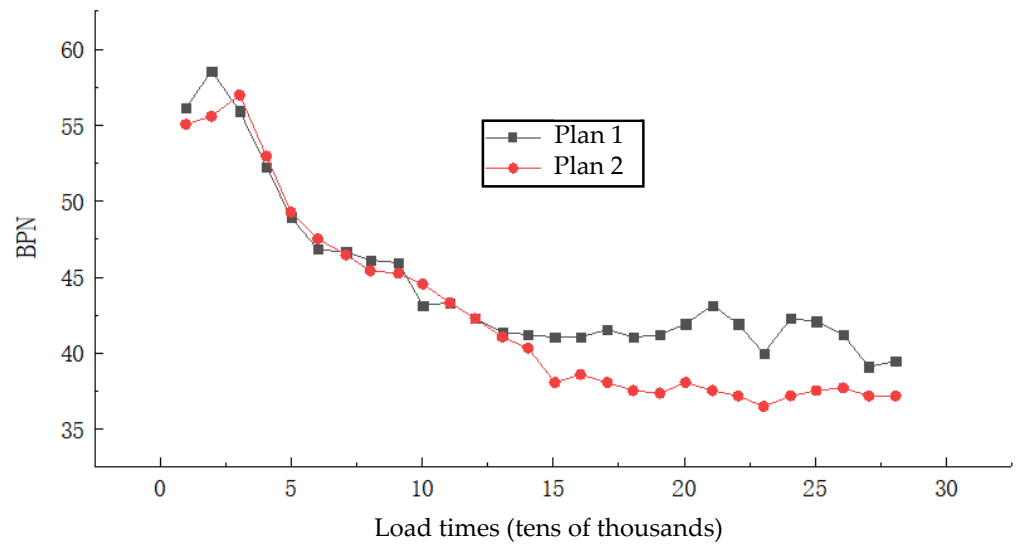


Figure 16. The friction coefficient of the road varies with the loading times.

The decay law of the pavement friction coefficient is in exponential form; hence, this study conducted regression on the decay law of the friction coefficient of Plan 1 and Plan 2 in logarithmic form, and the results are shown in Figure 17.

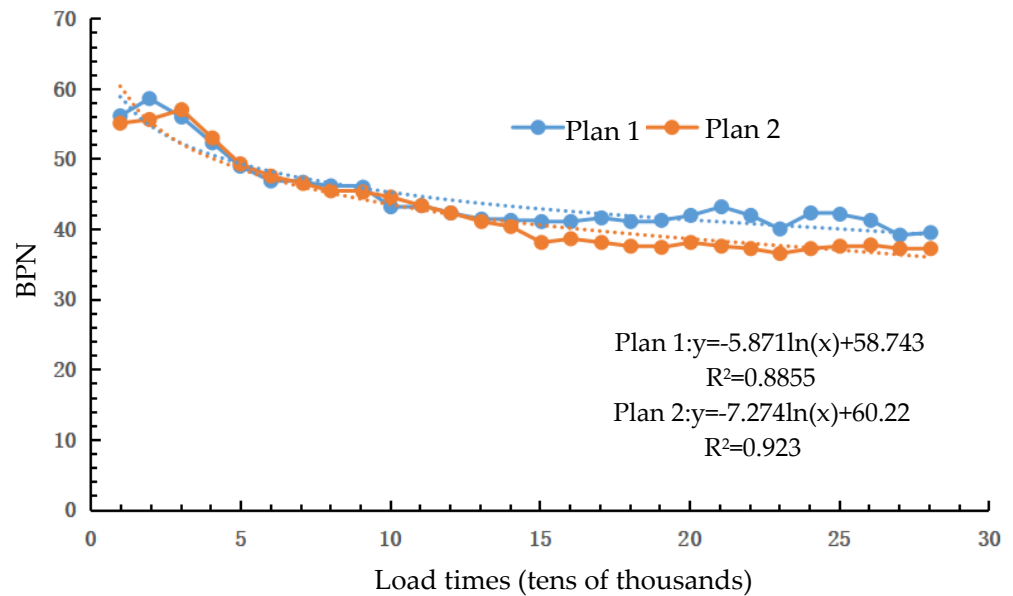


Figure 17. The fitting relationship between the road swing value and the number of loading times.

At first, the BPN values of Plan 1 and Plan 2 were similar. However, starting from about 150,000 times, Plan 1 exhibited a stronger anti-slip effect. The pavement material had a decisive influence on the surface shape of the pavement, and the angularity of the aggregate in the RAP material was reduced, which reduced the overall friction coefficient of the pavement.

3.1.3. Rutting Variation in Asphalt Pavement

The rutting development of pavement under different loading times was sorted and analyzed, as shown in Figure 18. There was a rapid development of rutting in the two types of road structure in the early stage. When the number of loadings reached 80,000, it changed towards slow development. The system entered the high-temperature stage at this point, and the development remained slow. The final rutting data for Plan 1 and

Plan 2 were 6 mm and 5.6 mm, respectively. Since the bottom layer of the two pavement structures on the test road was of the AC-20 recycled asphalt mixture with a RAP content of 25%, this indicates that the formation of rutting was due to the secondary compaction of the overall pavement structure and involved the small permanent plastic deformation of each pavement structural layer under the action of the load. In addition, the content of light oil in the aged asphalt in the hot asphalt pavement was reduced, which led to the increase in viscosity and the enhancement of compressive and shear resistance; therefore, the rut depth was less than that of ordinary recycled pavement.

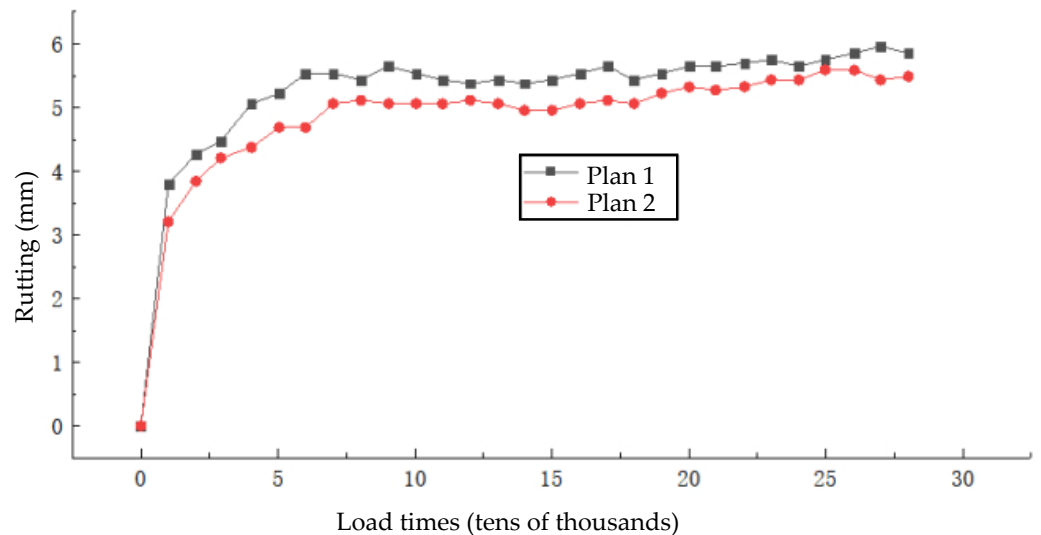


Figure 18. The variation in road rutting with loading times.

3.1.4. Strain Variation in Asphalt Pavement (Bottom Layer)

The strain corresponding to different loading times was monitored in real time, and the correlation curve results between the strain and loading times were obtained through analysis. These results are shown in Figure 19, where 2# and 5# are transverse sensors for Plan 1 and Plan 2, respectively, and 3# and 6# are longitudinal sensors for Plan 1 and Plan 2, respectively.

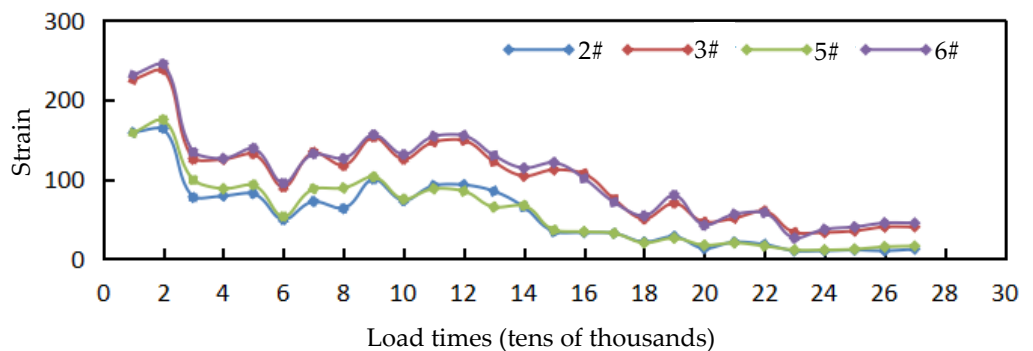


Figure 19. Relationship between the bottom strain and loading times.

Plan 1 and Plan 2 basically displayed the same strain law. When the loading times reached between 120,000 and 300,000, the environment entered the low-temperature stage. Therefore, the bottom strain turned to the sharply decreasing stage after 120,000 times, and the strain in this stage was affected more by temperature than by the loading times. These results indicated that the macroscopic mechanical responses and road service performances of the two pavement structures under load were basically the same, reflecting the good road performance of the recycled asphalt mixture.

3.2. Analysis of the Load–Deflection Relationship

3.2.1. Analysis of the Load–Deflection Relationship

The load and deflection data were analyzed, and the recycled asphalt mixture and ordinary asphalt mixture were compared and analyzed under different load frequencies and stress ratios. The specific relationship diagrams are shown in Figures 20–24.

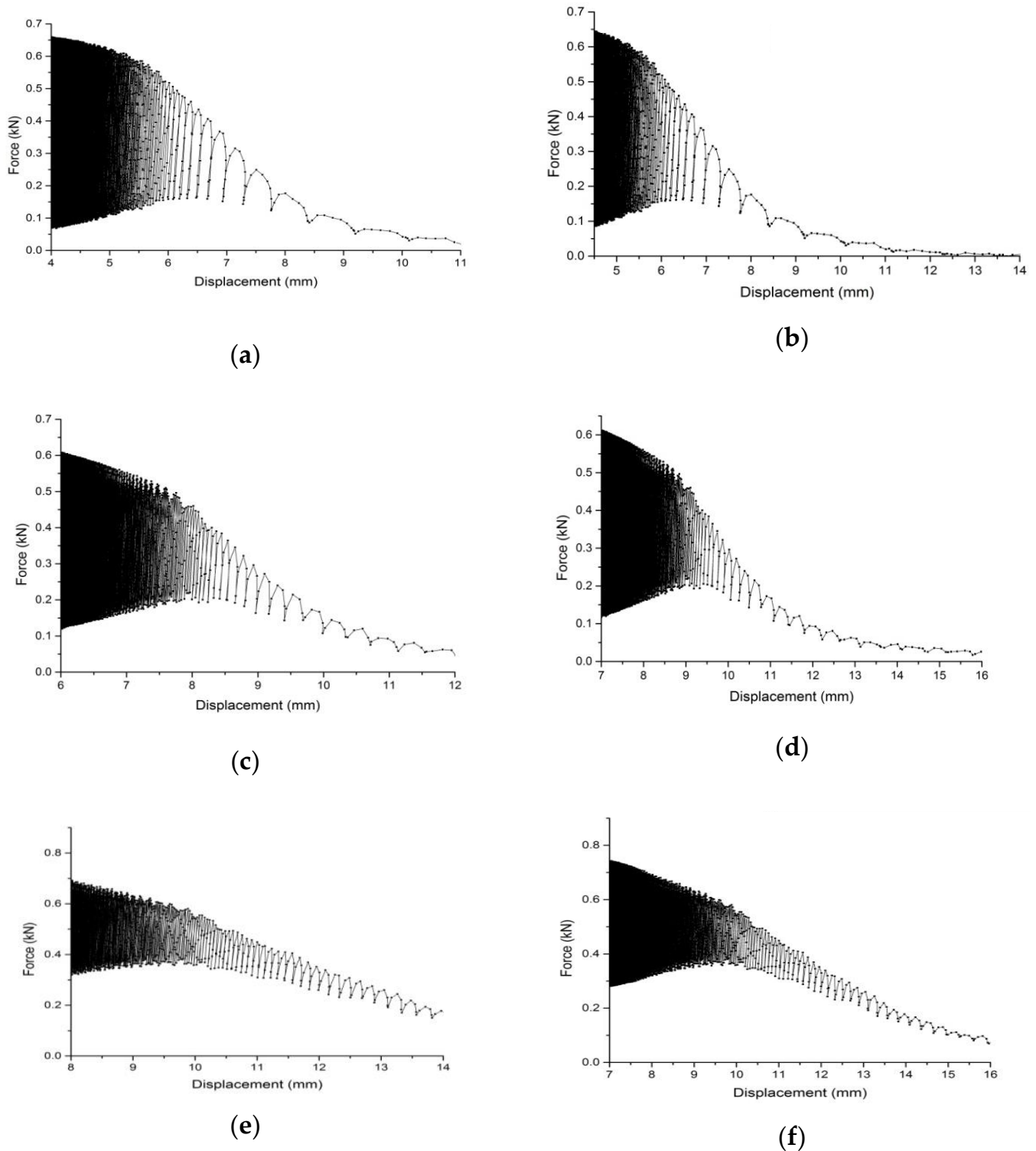
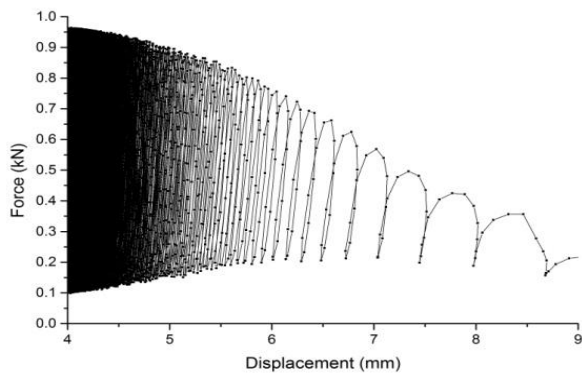
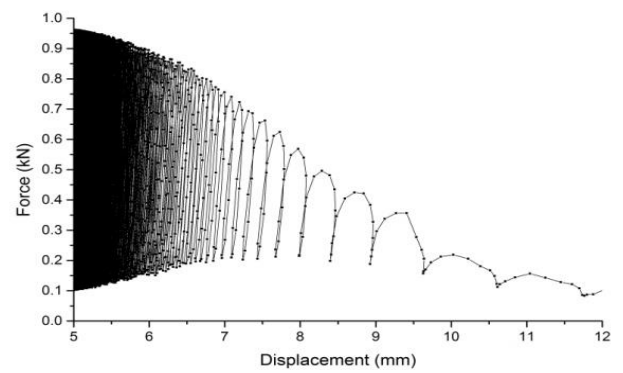


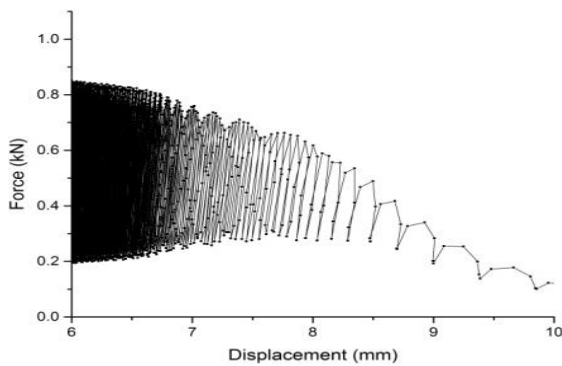
Figure 20. The relationship between load and deflection at different loading frequencies when the stress ratio was 0.2. (a) I-1 (5 Hz); (b) II-1 (5 Hz); (c) I-1 (10 Hz); (d) II-1 (10 Hz); (e) I-1 (20 Hz); and (f) II-1 (20 Hz).



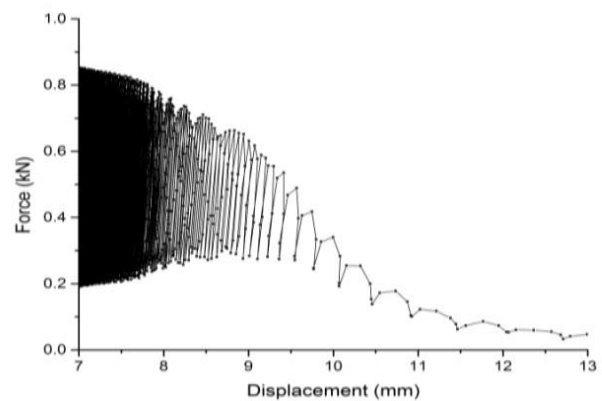
(a)



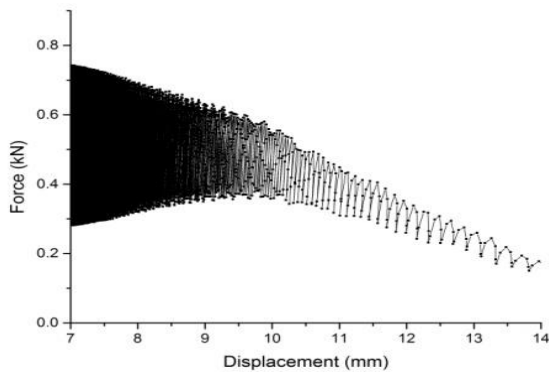
(b)



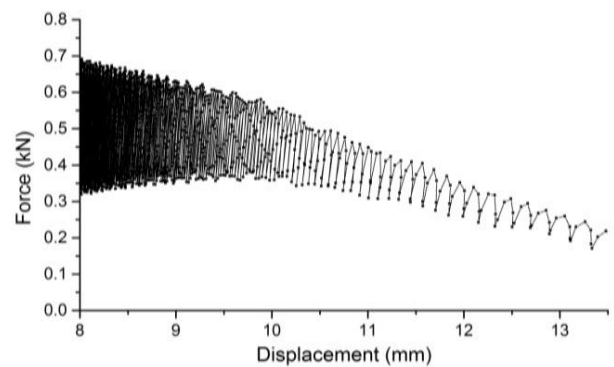
(c)



(d)



(e)



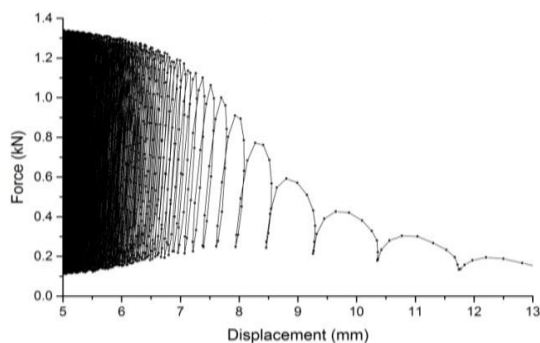
(f)

Figure 21. The relationship between load and deflection at different loading frequencies when the stress ratio was 0.3. (a) I-1 (5 Hz); (b) II-1 (5 Hz); (c) I-1 (10 Hz); (d) II-1 (10 Hz); (e) I-1 (20 Hz); and (f) II-1 (20 Hz).

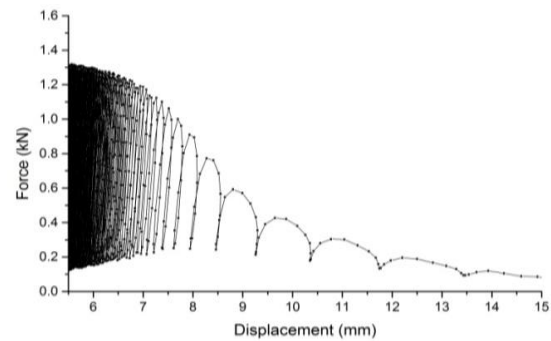
The following can be seen from Figures 20–24:

- (1) When the stress ratio was 0.2, 0.3, 0.4, 0.5, and 0.6, the failure forms of the ordinary asphalt mixture and the recycled asphalt mixture were basically the same under different loading frequencies. That is, in the process of repeated loading and unloading, the specimens' flexural deformation gradually accumulated until fractures occurred.

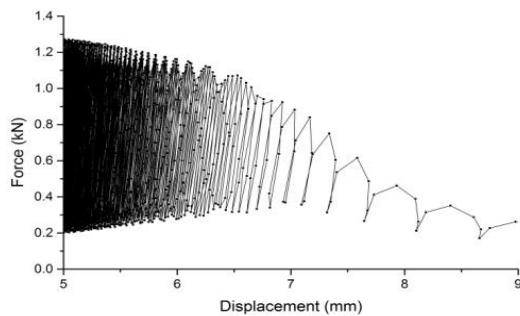
- (2) Under the same stress level and loading frequency, the curve relationships between load and deflection for the ordinary asphalt mixture and the recycled asphalt mixture were similar (basically consistent). The results showed that the fatigue performance of the recycled asphalt mixture can meet the requirements of ordinary asphalt mixture and meet the technical standards of asphalt pavement design.
- (3) The relationships between load and fatigue deformation for the ordinary asphalt mixture and the recycled asphalt mixture were different under different stress ratios and different loading frequencies. When the stress level was small (stress ratios of 0.2 and 0.3), the cumulative fatigue failure deformation of the ordinary asphalt mixture and the recycled asphalt mixture increased with the increase in loading frequency.
- (4) When the stress level was large (stress ratios of 0.4, 0.5, and 0.6), the cumulative fatigue failure deformation of the ordinary asphalt mixture and the recycled asphalt mixture decreased with the increase in loading frequency. The reason for this was that when the stress ratio was small, the flexural deformation of the trabecular specimen caused by the applied load was very small, far less than the bending and tensile failure limit deformation. Under high loading frequencies, the cumulative deformation of deflection increased faster, and the cumulative deformation of fatigue failure was larger. When the stress ratio was large, the load exerted great influence on the bending deformation of the trabecular specimen. The greater the loading frequency, the faster the time of action on the asphalt mixture viscoelastic specimen. The specimen was mostly elastomer, and the stiffness modulus was large. When the fatigue failure was reached, the cumulative deformation caused via fatigue failure was relatively small. However, under a certain stress level, due to the larger stiffness modulus, the flexural deformation will be relatively small, and fatigue cracking will not easily occur. Therefore, the higher the loading frequency of an asphalt mixture specimen, the greater the fatigue life.



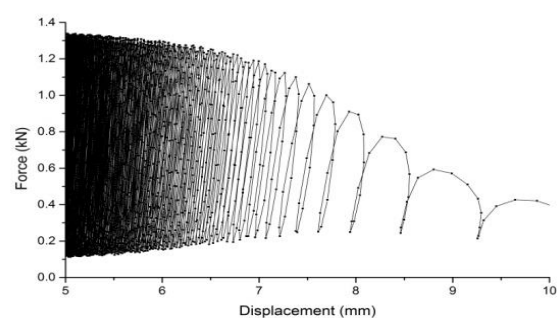
(a)



(b)



(c)



(d)

Figure 22. Cont.

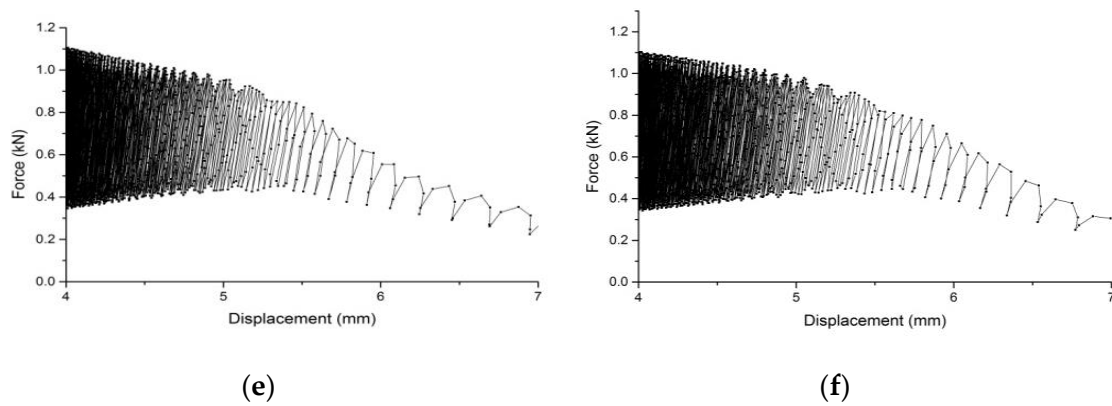


Figure 22. The relationship between load and deflection at different loading frequencies when the stress ratio was 0.4. (a) I-1 (5 Hz); (b) II-1 (5 Hz); (c) I-1 (10 Hz); (d) II-1 (10 Hz); (e) I-1 (20 Hz); and (f) II-1 (20 Hz).

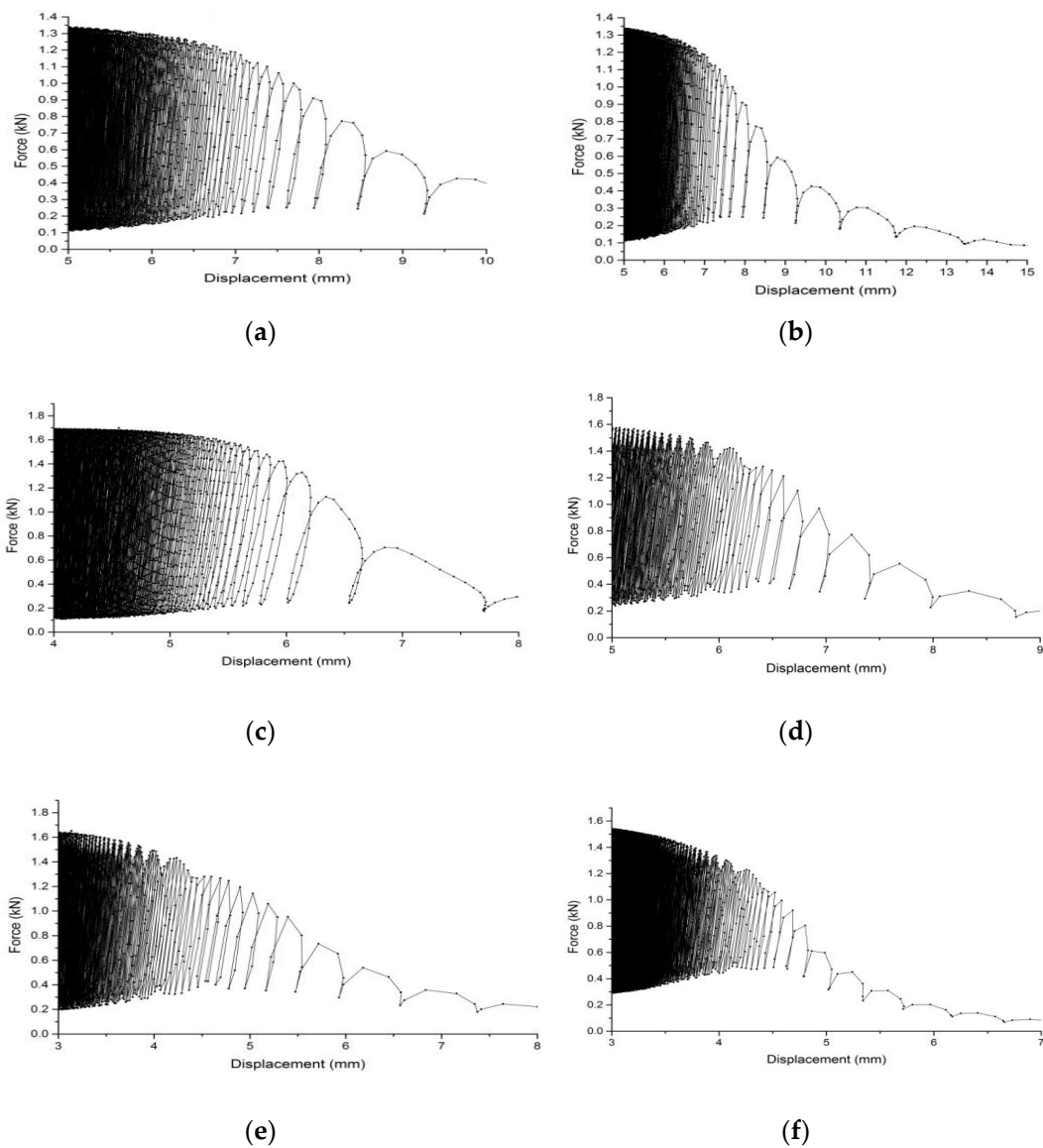


Figure 23. The relationship between load and deflection at different loading frequencies when the stress ratio was 0.5. (a) I-1 (5 Hz); (b) II-1 (5 Hz); (c) I-1 (10 Hz); (d) II-1 (10 Hz); (e) I-1 (20 Hz); and (f) II-1 (20 Hz).

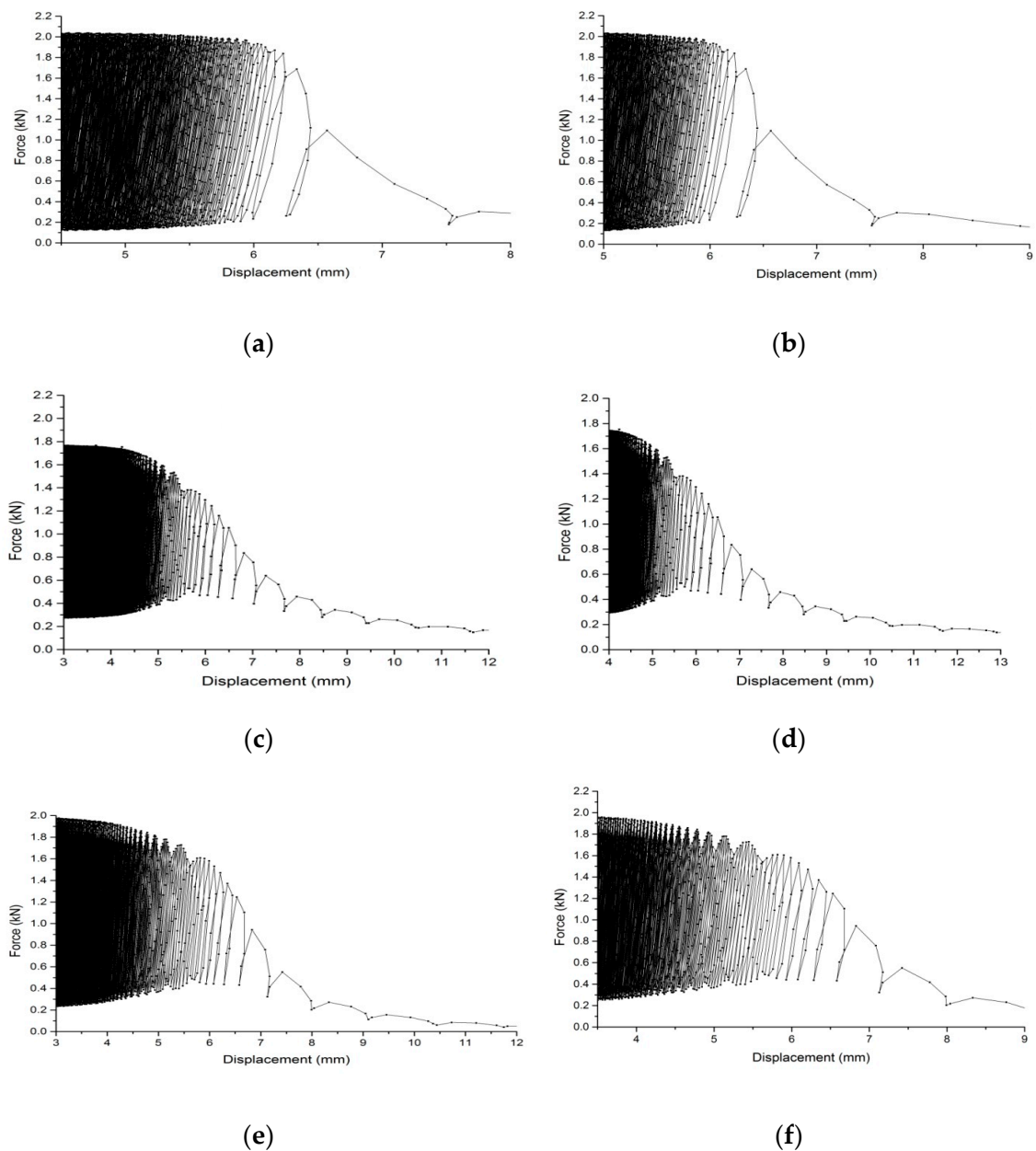


Figure 24. The relationship between load and deflection at different loading frequencies when the stress ratio was 0.6. (a) I-1 (5 Hz); (b) II-1 (5 Hz); (c) I-1 (10 Hz); (d) II-1 (10 Hz); (e) I-1 (20 Hz); (f) II-1 (20 Hz).

3.2.2. Three-Point Bending Fatigue Life Analysis

Figure 25 shows the three-point bending fatigue life data analysis, according to different load frequencies, and the different stress ratio comparative analysis.

Four stress levels of 0.3, 0.4, 0.5, and 0.6 were selected to carry out bending fatigue tests on the SMA-13 ordinary asphalt mixture, SMA-13 recycled asphalt mixture, and AC-20 recycled asphalt mixture at 5 Hz, 10 Hz, and 20 Hz, respectively. The following can be seen from Figure 25:

- (1) Under the same stress ratio, the fatigue life of II-1 and III-1 increased with the increase in loading frequency. When the stress ratio was 0.3, the fatigue life difference between the asphalt mixtures with loading frequencies of 5 Hz and 10 Hz was not obvious, but the fatigue life of the asphalt mixture with a loading frequency of 20 Hz was 3.8 times than that of the 5 Hz mixture and 3.1 times than that of the 10 Hz mixture.

This indicates that the influence of higher loading frequency on the fatigue life of an asphalt mixture is more obvious when other test conditions are the same. Under the same test conditions, the order of fatigue life of the recycled asphalt mixtures under different loading frequencies was 20 Hz > 10 Hz > 5 Hz.

- (2) Under most of the same test conditions, the fatigue life of I-1 and II-1 was similar. This indicates that the recycled asphalt mixture met the requirements for long-term use of asphalt pavement. Although the aging of the RAP material in the recycled asphalt mixture has adverse effects on the fatigue life, the addition of a regenerant can better restore the pavement performance of the aged asphalt, thus improving the fatigue life of the recycled asphalt mixture.
- (3) Under the same loading frequency, the fatigue life significantly decayed with the increase in stress ratio, which indicates that the stress ratio has a major effect on the fatigue life of an asphalt mixture. When the loading frequency was 20 Hz, with the increase in stress ratio from 0.3 to 0.6, the fatigue life of I-1 decreased by 66.3%, 85.3%, and 94.8%, and the fatigue life of II-1 decreased by 65.5%, 85.8%, and 95.1%. As the stress ratio gradually increased, the applied load was closer to the ultimate stress of bending and tensile failure of the specimen. With the increase in load times, the residual deformation of the specimen gradually increased, the stiffness (or modulus) of the material gradually decreased, the micro-cracks continuously developed, and, finally, the complete fracture occurred.

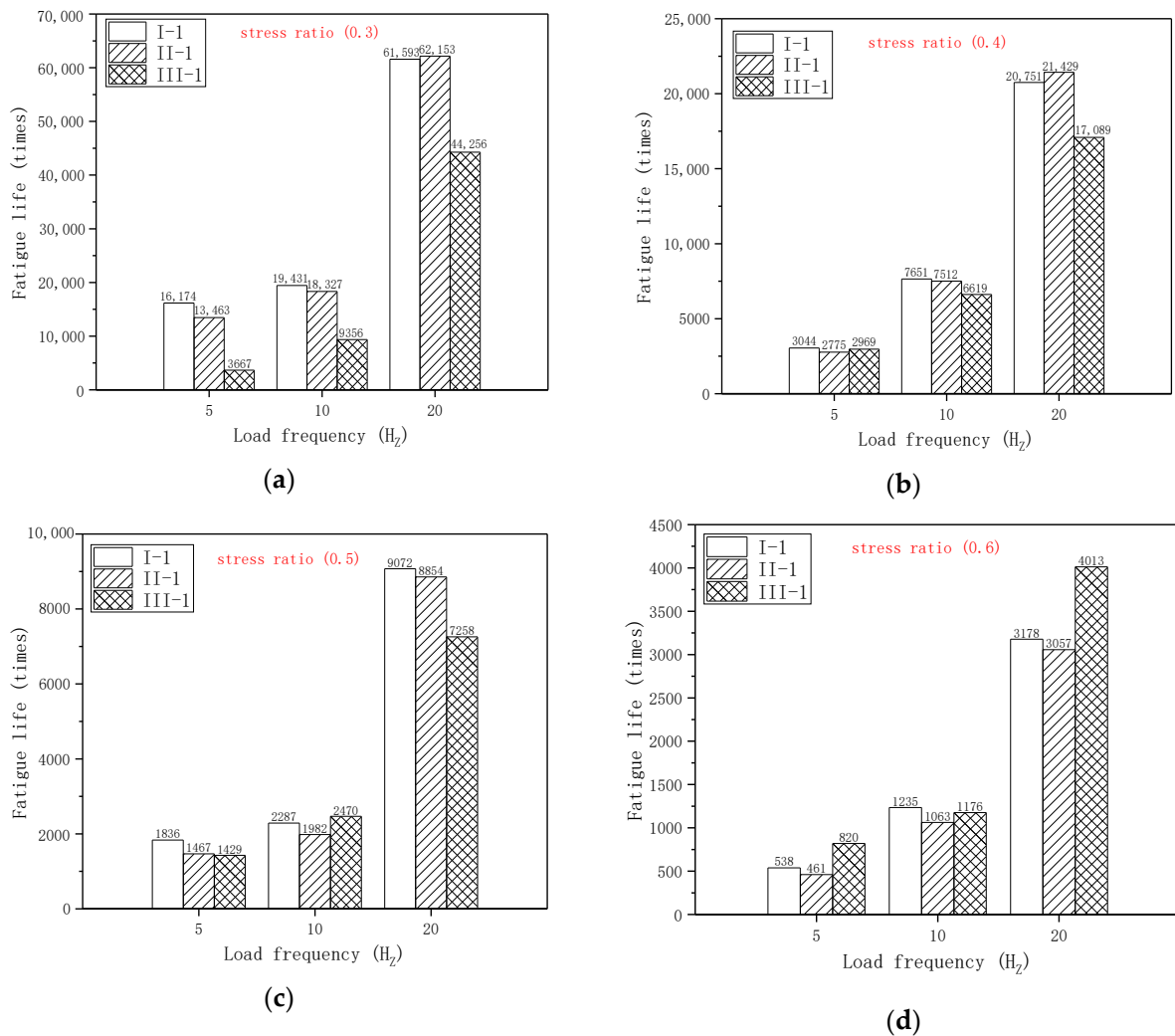


Figure 25. Relationship between load frequency and fatigue life under different stress ratios. (a) Stress ratio of 0.3. (b) Stress ratio of 0.4. (c) Stress ratio of 0.5. (d) Stress ratio of 0.6.

3.2.3. Fatigue Equation under Stress Control Mode

The test load level represents the load borne by the real road surface to some extent. According to the analysis of relevant data at home and abroad, five stress levels of 0.2, 0.3, 0.4, 0.5, and 0.6 were selected to replace the ordinary load and heavy load of different traffic axles. This experiment simulated different vehicle speeds on the road under the three loading frequencies of 5 Hz, 10 Hz, and 20 Hz. In accordance with a large number of experimental studies, it can be verified from the figure that the stress ratio and fatigue life showed a good linear relationship on the single logarithmic curve, which can be expressed via Formula (1):

$$\lg N_f = k + n \times S_i \tag{1}$$

where N_f is the number of times the load is applied; that is, the fatigue life; S_i is the stress ratio; k ; and n is the regression constant.

At 15 °C, the stress ratio and fatigue life of the SMA-13 recycled asphalt mixture under the three loading frequencies of 5 Hz, 10 Hz, and 20 Hz showed linear regression, and the single logarithmic fatigue equation was obtained, as shown in Figures 26 and 27.

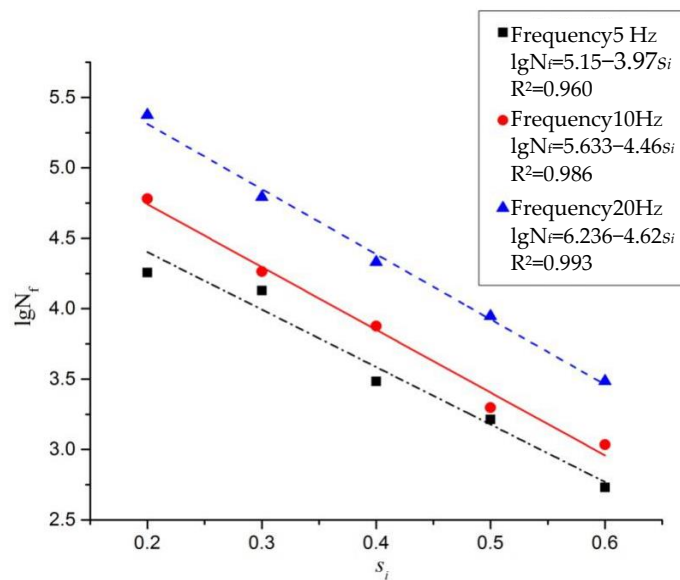


Figure 26. Stress ratio–fatigue curve of II-1.

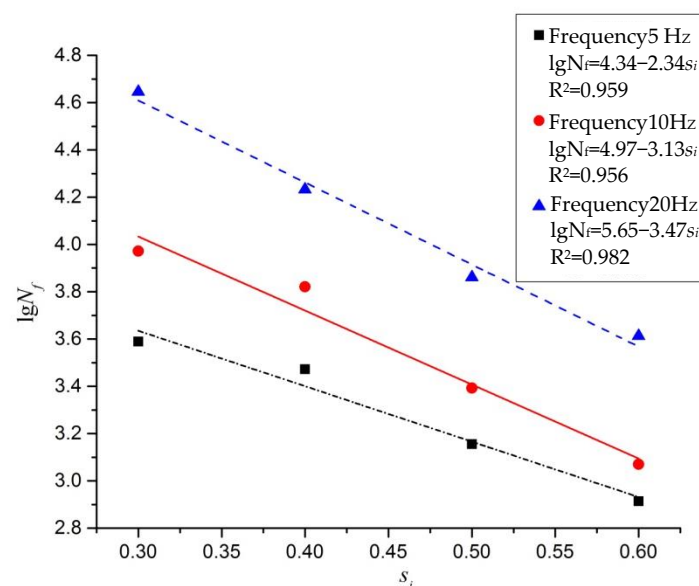


Figure 27. Stress ratio–fatigue curve of III-1.

As can be seen from Figures 26 and 27, the fatigue equations under different loading frequencies were basically parallel. The stress level had a significant effect on the fatigue life. With the increase in stress level, the fatigue life of the recycled asphalt mixture gradually decreased. The n value in the fatigue equation for the SMA-13 recycled asphalt mixture ranged from 3.97 to 4.62, and the variation range was relatively small. It was shown that the loading frequency had little difference in the sensitivity of the fatigue life and stress level of the recycled asphalt mixture specimens. The n value in the fatigue equation for the AC-20 recycled asphalt mixture ranged from 2.34 to 3.47, and the variation range was relatively large. This indicates that the loading frequency was more sensitive to the fatigue life and stress level of the specimen. The intercept (k) of the fatigue equation for the SMA-13 recycled asphalt mixture ranged from 5.15 to 6.236, and that of the AC-20 recycled asphalt mixture ranged from 4.34 to 5.65, with a relatively large variation range. This indicates that there were two kinds of grading regeneration under three kinds of load frequency differences between the fatigue performances of the recycled asphalt mixture.

For the indoor small bending fatigue test, the loading frequency of the test load was selected considering the actual vehicle load action time and determined according to Vander Poel's Formula (2):

$$t = \frac{1}{2\pi f} \quad (2)$$

where t is the loading time and f is the loading frequency.

Therefore, the larger the loading frequency of the trabecular specimen, the shorter the actual vehicle loading time, and the faster the vehicle running speed. The asphalt mixture at room temperature was viscoelastic. As the loading frequency increased, the action time on the asphalt mixture viscoelastic specimens was faster, and the specimens were mostly elastomer with a larger stiffness modulus. At a certain stress level, the bending and tensile deformation was relatively small, and it was not easy to produce fatigue cracking. Therefore, the higher the loading frequency of the recycled asphalt mixture specimen, the greater the fatigue life.

3.3. Dynamic Modulus Analysis of the Asphalt Mixture Based on the Test Road

Dynamic modulus tests were carried out on the ordinary SBS-modified asphalt mixture and the SBS-modified recycled asphalt mixture before and after wheel loading, and the test results are shown in Figures 28–30.

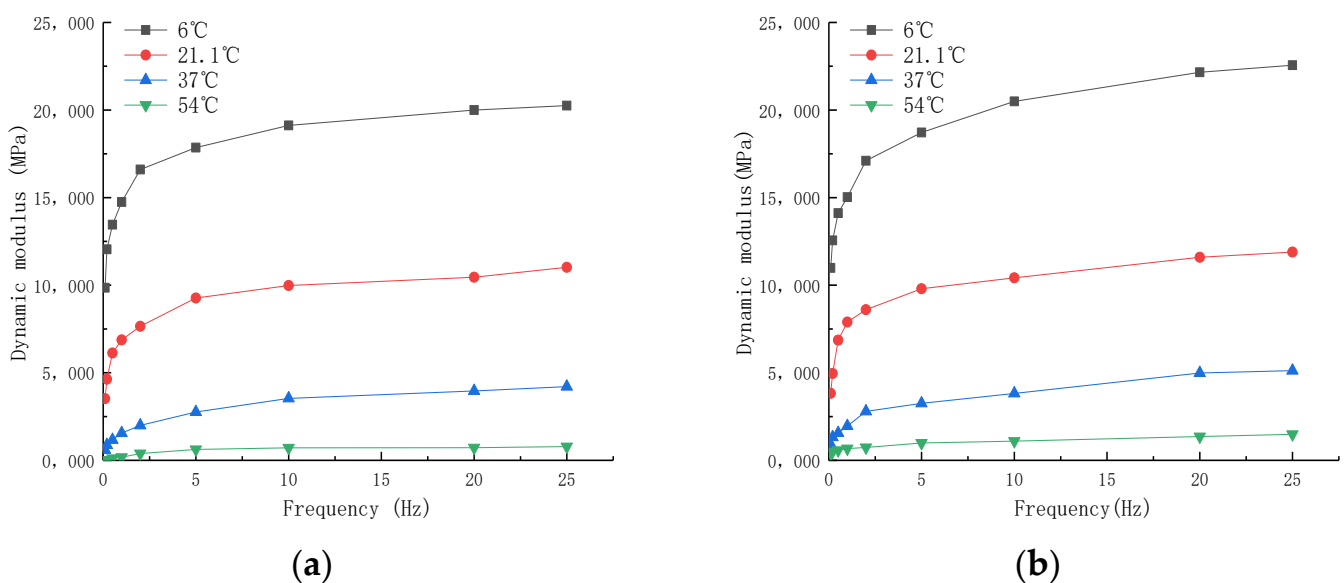


Figure 28. Dynamic modulus of the ordinary SMA-13 asphalt mixture. (a) The dynamic modulus of I-1. (b) The dynamic modulus of I-2.

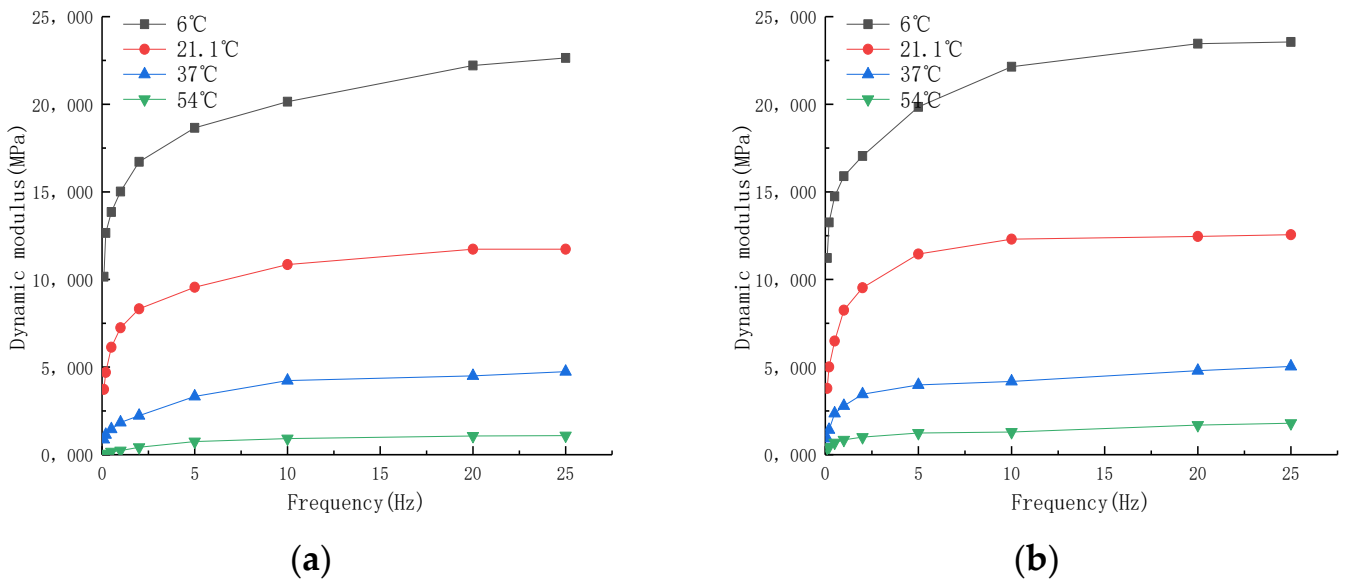


Figure 29. Dynamic modulus of the SMA-13 recycled asphalt mixture. (a) The dynamic modulus of II-1. (b) The dynamic modulus of II-2.

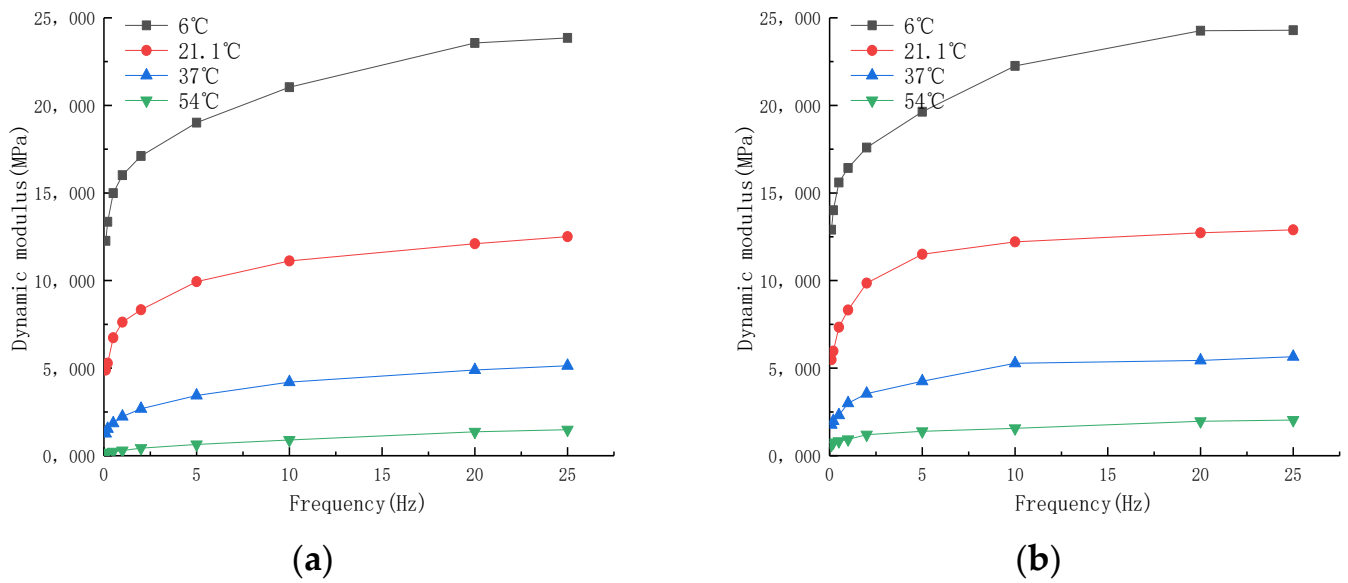


Figure 30. Dynamic modulus of the AC-20 recycled asphalt mixture. (a) The dynamic modulus of III-1. (b) The dynamic modulus of III-2.

- (1) The dynamic modulus of the asphalt mixture material increased with the increase in load frequency under the same temperature condition, but with the continuous increase in temperature, the dynamic modulus gradually decreased the growth rate until it approached a quantitative value. The dynamic modulus of the asphalt mixture rapidly increased before 3 Hz and then tended to gradually slow down. Therefore, the dynamic modulus of the asphalt mixture will not become infinitely higher due to the increasing frequency, as when the loading frequency continues to increase, the viscosity of the asphalt mixture will gradually decrease, and its elasticity will gradually increase.
- (2) Based on the ALT full-scale experiment, it was found that under the same temperature conditions, the dynamic elastic modulus of the asphalt mixture before the equipment wheel load was greater than that after the wheel load. The reason for this is that after long-term wheel loading, the fine aggregate will be compacted, the coarse aggregate

- will be crushed, and the asphalt will age, which will lead to the structural stiffness and dynamic modulus of the mixed material being reduced.
- (3) The modulus of the SMA-13 recycled asphalt mixture was smaller than that of the AC-20 recycled asphalt mixture. Structurally speaking, SMA-13 is characterized by discontinuous gradation, with more coarse aggregates and less fine aggregates, and its mixture belongs to the skeleton compact structure. AC is characterized by continuous gradation, a continuous amount of each file material, and step-by-step gap filling, and its mixed material structure belongs to the suspension dense type. This is the cause of the smaller modulus of the former and the larger modulus of the latter.
 - (4) The dynamic modulus of the asphalt mixture increased at temperature and rapidly decreased at different loading frequencies. When the test temperature was different, the dynamic modulus of the asphalt mixture increased with the increase in loading frequency. At the same frequency, the dynamic modulus decreased with the increase in temperature, which was due to the gradual decrease in the resilience modulus of asphalt as a binder. It can be seen that the basic mechanical properties of a viscoelastic asphalt mixture can be accurately reflected through dynamic modulus testing.
 - (5) The modulus of the recycled asphalt mixture was slightly larger than that of the ordinary asphalt mixture, which was because the recycled asphalt mixture was mixed with 20% RAP material, and the elastic modulus became larger due to the existence of the RAP material. Under different temperatures and frequencies, the dynamic modulus of the SMA-13 ordinary asphalt mixture and SMA-13 recycled asphalt mixture after accelerated loading were close to each other, which is consistent with the residual fatigue life rule of the two given in Section 3.2, and the same was true for the AC-20 recycled asphalt mixture.

3.4. Analysis of Asphalt Secondary Aging Components

The four-component test data of asphalt after secondary aging were compared and analyzed, as shown in Figures 31 and 32.

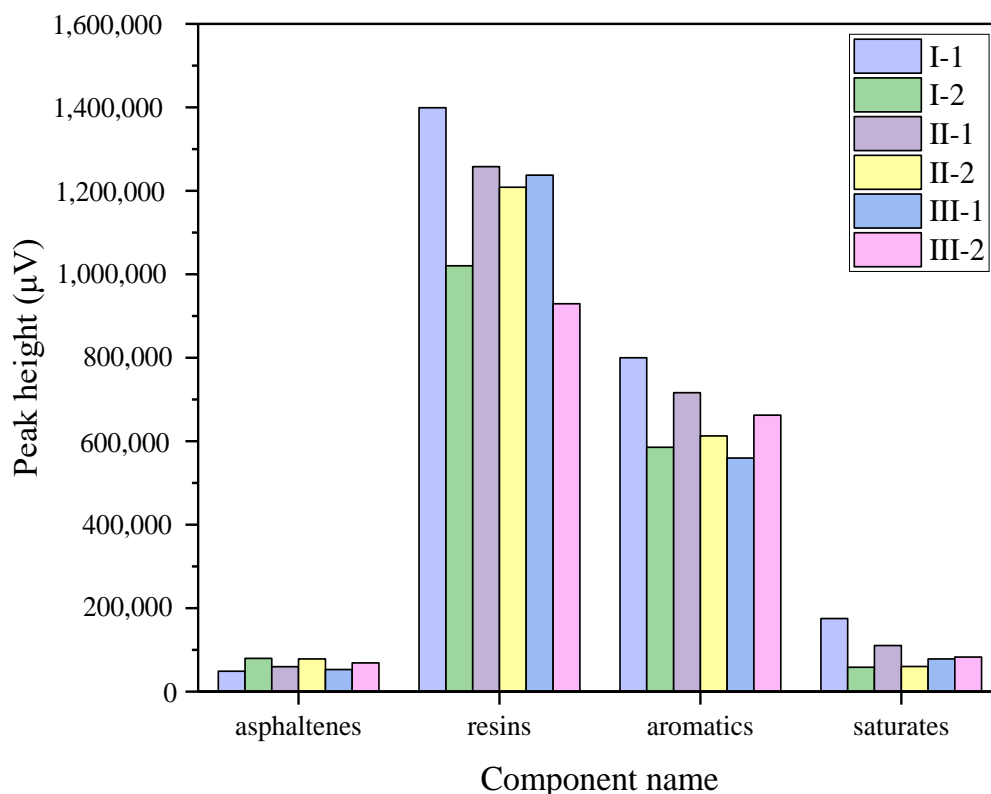


Figure 31. Peak heights of the four components of different asphalt mixtures.

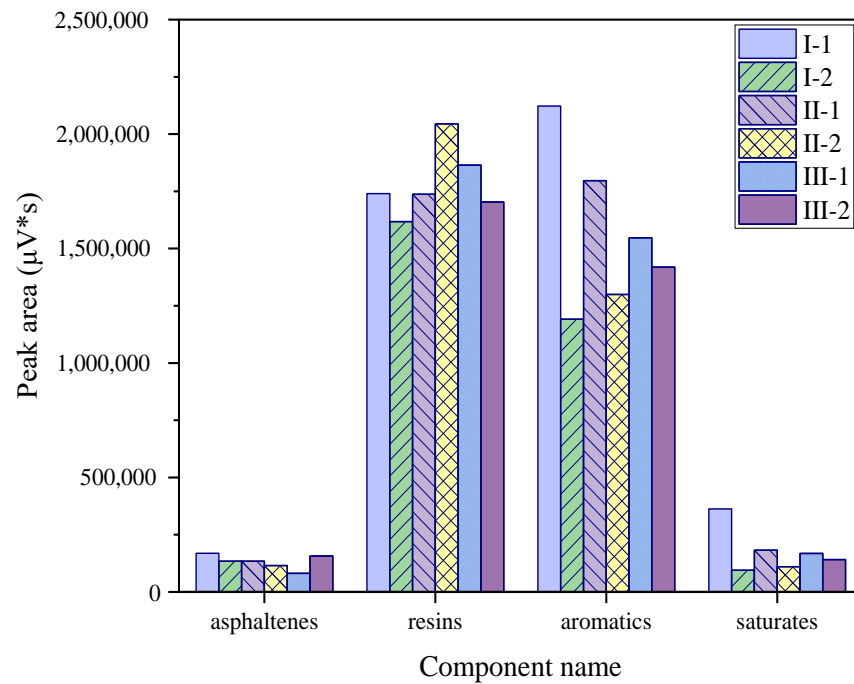


Figure 32. Peak areas of the four components of different asphalt mixtures.

The contents of each component (saturates, aromatics, resins, and asphaltenes) in the sample, W_i , were calculated according to Formulas (3) and (4):

$$W_i = (A_i/A) \times 100\% \tag{3}$$

$$A = \sum A_i \tag{4}$$

where W_i is the content of a component in the standard sample, A_i is the corrected peak area of a component in the sample, and A is the total peak area of each component in the standard sample.

The specific test data statistics according to Formulas (3) and (4) are shown in Figure 33.

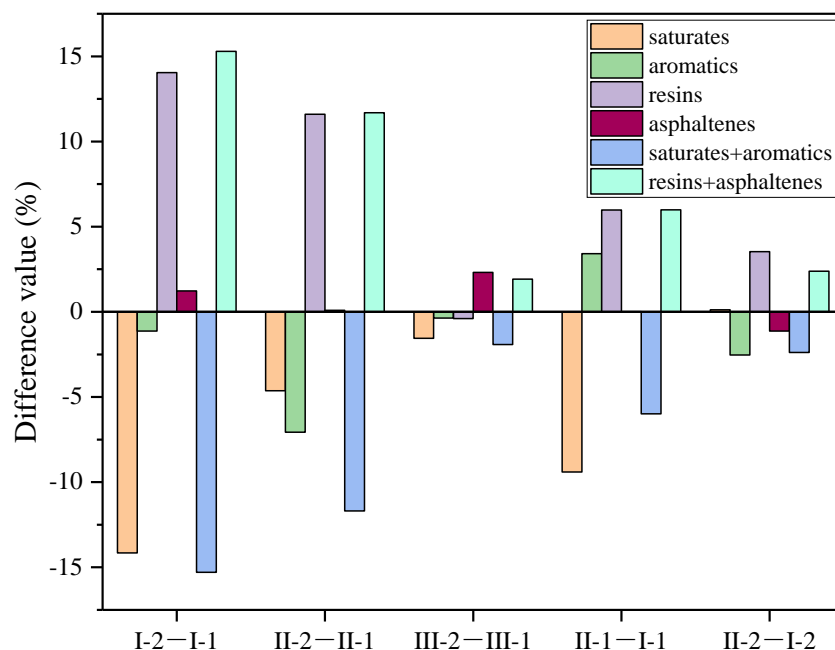


Figure 33. Contents of four components in different types of asphalt mixtures.

- (1) Under accelerated loading, different loads under the same thermal oxygen, light, and water conditions will have different influences on the pavement over a period of time. According to the experimental data, the saturates + aromatics content of I-2 was 58.74%, and the saturates + aromatics content of I-1 was 74.03%, with I-2 < I-1. The resins + asphaltenes content of I-2 was 41.26%, and the resins + asphaltenes content of I-1 was 25.97%. The saturates and aromatics of asphalt following the accelerated loading section were reduced, and the lighter components were converted more into resins and asphaltenes. Under the coupling action of load, hot oxygen, light, and water, the aging of asphalt was accelerated, and the aging degree was normal, without serious aging phenomena.
- (2) The saturates + aromatics content of II-2 was 56.35%, and the content of saturates + aromatics of II-1 was 11.69% more than II-2. The contents of resins + asphaltenes under un-accelerated loading and accelerated loading were 31.96% and 43.65%, respectively. Under the coupling action of running load, hot oxygen, light, and water, certain aging conditions were generated, but no serious aging phenomena occurred.
- (3) The content of saturates + aromatics in II-1 was 5.99% less than that in I-1, and the content of saturates + aromatics in II-2 was 2.39% less than that in I-2. Based on the content of the four components, there were no excessive aging phenomena in the recycled asphalt mixture. After the fatigue test, the contents of each component in the recycled asphalt mixture after aging were basically the same as that of the ordinary asphalt mixture. This may be because the recycled asphalt mixture contains RAP, which has undergone aging and has stable content of light components. The old and new asphalt were combined and the four components were recombined, and the content of light components of I-1 was 5.99% different from that of I-1. After accelerated loading, the light component content of II-2 was 2.39% different from that of I-2, and the light components of II-2 and II-1 were only 11.69% lower. Therefore, the recycled asphalt mixture exhibited better fatigue resistance under the same aging conditions. The road performance and durability of the recycled asphalt mixture met the application requirements.
- (4) Distinct from the accelerated loading of the SMA-13 ordinary asphalt mixture and SMA-13 recycled asphalt mixture on the upper layer, the different components of the AC-20 recycled asphalt mixture on the bottom layer displayed little difference under the two conditions of accelerated loading and unaccelerated loading. The saturates + aromatics content of III-2 was 62.59%, while the saturates + aromatics content of III-1 was 64.51% (basically the same). The resins + asphaltenes content of III-2 was not different from that of III-1. This indicated that the aging degree of the accelerated loading section and the unaccelerated loading section in the following layer were basically the same, with no obvious change, and that the road performance and durability met the use requirements. After accelerated loading, the light component of the SMA-13 thermal reclaimed asphalt mixture decreased by 11.39%, and that of the AC-20 thermal reclaimed asphalt mixture by 1.92%, mainly because the full-scale experiment directly acted on the upper layer, and the influence of the thermal oxygen, light, and water conditions also mainly acted on the upper layer. However, the AC-20 thermal reclaimed asphalt mixture was located at the bottom layer of the pavement structure, which was less affected and did not experience accelerated asphalt aging.

4. Conclusions

In this study, a series of tests were carried out to evaluate the decay mechanisms and rules of recycled asphalt pavement using a full-scale experiment. The following conclusions can be drawn from the tests:

- (1) As the number of loading times increases, the BPN value of the two structures tended to be stable, and the BPN of Plan 2 was six lower than that of Plan 1. On the basis of the full-scale experiment, the recycled asphalt mixture and ordinary asphalt mixture exhibited good road performance. However, the ordinary asphalt mixture pavement

had better skid resistance. As the bottom layer, each component of the AC-20 recycled asphalt mixture showed little difference after accelerated loading and unaccelerated loading and remained consistent. This indicated that accelerated loading aging mainly affects the upper layer of pavements. In summary, recycled asphalt mixtures should not be applied to the upper layer of pavements but can be rationalized in the middle layer and the bottom layer of pavements.

- (2) Under the same stress level and loading frequency, the curve relationships between load and deflection for the SMA-13 and AC-20 ordinary asphalt mixtures and the recycled asphalt mixture were similar (basically consistent). The results showed that the fatigue performance of a recycled asphalt mixture can meet the requirements of an ordinary asphalt mixture and meet the technical standards of asphalt pavement design. The macroscopic mechanical response and road service performance of the two pavement structures under load were basically the same, which reflects the good road performance of the blended recycled asphalt mixture.
- (3) When the stress ratio was 0.3, the fatigue life difference between the asphalt mixtures with loading frequencies of 5 Hz and 10 Hz was not obvious, but the fatigue life of the asphalt mixture with a loading frequency of 20 Hz was 3.8 times than that of the 5 Hz mixture and 3.1 times than that of the 10 Hz mixture. Under the same test conditions, the order of fatigue life of the recycled asphalt mixtures under different loading frequencies was 20 Hz > 10 Hz > 5 Hz.
- (4) The stress ratio and fatigue life showed a good linear relationship on the single logarithm curve, and the fatigue equations for the recycled asphalt mixtures under different load frequencies were obtained; that is, $\lg N_f = k + n \times S_i$. The n value of AC-20 ranged from 2.34 to 3.47, and the variation range was relatively large, indicating that the loading frequency was more sensitive to the fatigue life and stress level of the specimens.
- (5) The saturates and aromatics of asphalt in the accelerated loading section were decreased, while the light components were transformed more into resins and asphaltenes. Following the full-scale experiment, the light component of the SMA-13 recycled asphalt mixture decreased by 11.69%, while that of the SMA-13 ordinary asphalt mixture decreased by 15.29%, indicating that the coupling effect of load, thermal oxygen, light, and water accelerated the aging of the asphalt, but no serious aging phenomena occurred. The recycled asphalt mixture exhibited better fatigue resistance under the same aging conditions.
- (6) The pendulum tribometer used in this study could not fully simulate tire contact with the road, as real vehicle tires are much rougher and can provide better grip on the road surface. It is well known that BPN measurements are more influenced by non-slip micro-texture components than by macroscopic texture. This problem may lead to slight changes in the BPN value, especially when the sample surface void is blocked by dust or the road is wet in rainy days, and the BPN cannot be accurately detected. In addition, temperature, load, light, water, and other factors have a great impact on pavement aging. Therefore, it is necessary to monitor the road temperature, load, and other parameters and comprehensively analyze the decay mechanisms and laws of recycled asphalt pavement from a multi-directional perspective, so as to improve the utilization rate of recycled materials to make full use of resources and reduce waste.

Author Contributions: Conceptualization, J.G.; methodology, J.G. and Q.X.; design of analysis, Q.X. and Q.Z.; data curation, Q.Z., Q.S. and K.S.; validation, B.X.; writing—original draft, Q.X., Q.S. and Z.Y.; writing—review and editing, J.G. and Q.X. All authors have read and agreed to the published version of the manuscript.

Funding: This research was funded by the 2023 Shandong Provincial Transportation Science and technology plan, (Contract number: 2023B26).

Institutional Review Board Statement: Not applicable.

Informed Consent Statement: Not applicable.

Data Availability Statement: All of the data used to support the results of this study can be obtained from the corresponding authors according to the requirements.

Acknowledgments: The authors would like to thank the Shandong Transportation Service Center and the Shandong Transportation Institute for their financial support and technical services for this research work.

Conflicts of Interest: The authors declare no conflict of interest.

References

1. Ruiz, A.; Guevara, J. Sustainable Decision-Making in Road Development: Analysis of Road Preservation Policies. *Sustainability* **2020**, *12*, 872. [\[CrossRef\]](#)
2. Roach, P.E.; Ugursal, I. Development and technoeconomic evaluation of pathways to new construction net-zero energy houses in Nova Scotia. *Trans. Can. Soc. Mech. Eng.* **2020**, *45*, 221–232. [\[CrossRef\]](#)
3. Perumal, L.; New, M.; Jonas, M.; Liu, W. The impact of roads on sub-Saharan African ecosystems: A systematic review. *Environ. Res. Lett.* **2021**, *16*, 113001. [\[CrossRef\]](#)
4. Sidle, R.C. Dark Clouds over the Silk Road: Challenges Facing Mountain Environments in Central Asia. *Sustainability* **2020**, *12*, 9467. [\[CrossRef\]](#)
5. Suprayoga, G.B.; Witte, P.; Spit, T. Coping with strategic ambiguity in planning sustainable road development: Balancing economic and environmental interests in two highway projects in Indonesia. *Impact Assess. Proj. Apprais.* **2020**, *38*, 233–244. [\[CrossRef\]](#)
6. Zhao, H.; Su, J.; Ma, S.; Su, C.; Wang, X.; Li, Z.; Wei, J.; Cui, S. Study on Cold Recycled Asphalt Mixtures with Emulsified/Foamed Asphalt in the Laboratory and On-Site. *Coatings* **2022**, *12*, 1009. [\[CrossRef\]](#)
7. Li, J.; Zhu, L.; Yu, M.; Zuo, S.; Cui, X.; Liu, P. Long-Term Performance of Recycled Asphalt Pavement with Recycled Engine Oil Bottom Based on Accelerated Loading Test. *Coatings* **2022**, *12*, 522. [\[CrossRef\]](#)
8. Li, M.; Tang, W.; Yu, X.; Zhan, H.; Wang, X.; Wang, Z. Laboratory investigation on blending process of reclaimed asphalt mixture. *Constr. Build. Mater.* **2022**, *325*, 126793. [\[CrossRef\]](#)
9. Li, X.; Wang, Q.; Liu, S. Research on Application of Warm Mix Asphalt Technology in Hot In-Place Recycled Engineering. *Appl. Mech. Mater.* **2013**, *361–363*, 1655–1658. [\[CrossRef\]](#)
10. Reza, I.; Luis, L.; Alan, C. Integrated performance evaluation of asphalt mixtures with very high reclaimed asphalt pavement (RAP) content. *Constr. Build. Mater.* **2022**, *347*, 129607. [\[CrossRef\]](#)
11. Yin, P.; Pan, B. Effect of RAP content on fatigue performance of hot-mixed recycled asphalt mixture. *Constr. Build. Mater.* **2022**, *328*, 127077. [\[CrossRef\]](#)
12. Marcandré, B.; Sébastien, L.; Kevin, B.; Alan, C. Laboratory Study of the Effects of the Mixer Type and Mixing Time on the Volumetric Properties and Performance of a HMA with 30 Percent Reclaimed Asphalt Pavement. *Materials* **2023**, *16*, 1300. [\[CrossRef\]](#)
13. Li, F.; Zhu, H.; Yan, J.; Liu, Q.; Zhang, Z. Experimental Study of Hot Recycled Asphalt Mixtures with High Percentages of Reclaimed Asphalt Pavement and Different Recycling Agents. *J. Test. Eval.* **2014**, *42*, 1183–1190.
14. Gao, J.; Yao, Y.; Huang, J.; Yang, J.; Song, L.; Xu, J.; Lu, X. Effect of Hot Mixing Duration on Blending, Performance, and Environmental Impact of Central Plant Recycled Asphalt Mixture. *Buildings* **2022**, *12*, 1057. [\[CrossRef\]](#)
15. Prospero, E.; Bocci, E.; Bocci, M. Effect of Bitumen Production Process and Mix Heating Temperature on the Rheological Properties of Hot Recycled Mix Asphalt. *Sustainability* **2022**, *14*, 9677. [\[CrossRef\]](#)
16. Bocci, E.; Bocci, M.; Prospero, E. Influence of the Hot-Mix Asphalt Production Temperature on the Effectiveness of the Reclaimed Asphalt Rejuvenation Process. *Infrastructures* **2022**, *8*, 8. [\[CrossRef\]](#)
17. Cong, P.; Zhang, Y.; Liu, N. Investigation of the properties of asphalt mixtures incorporating reclaimed SBS modified asphalt pavement. *Constr. Build. Mater.* **2016**, *113*, 334–340. [\[CrossRef\]](#)
18. Homsy, F.; Bodin, D.; Yotte, S.; Breysse, D.; Balay, J.M. Fatigue life modelling of asphalt pavements under multiple-axle loadings. *Road Mater. Pavement Des.* **2012**, *13*, 749–768. [\[CrossRef\]](#)
19. Dong, C.; Liu, W.; Zhou, L.; Zhang, R.; Kan, Q.; Leng, W. Evaluation on Fatigue Life of Expressway Asphalt Pavement Based on Tire-Pavement-Subgrade Coupling Model. *Am. J. Civ. Eng.* **2017**, *5*, 400–407.
20. Ziari, H.; Aliha, M.; Mojaradi, B.; Jebalbarez, S. Investigating the effects of loading, mechanical properties and layers geometry on fatigue life of asphalt pavements. *Fatigue Fract. Eng. Mater. Struct.* **2019**, *42*, 1563–1577. [\[CrossRef\]](#)
21. Yu, Y.; Tang, S.; Xu, G.; Fan, Y.; Wu, Y.; Wang, H.; Yang, J. Investigations on the long-term skid resistance of epoxy asphalt mixture based on accelerated loading test. *Constr. Build. Mater.* **2023**, *365*, 130150. [\[CrossRef\]](#)
22. Hoha, D.; Boboc, V.; Boboc, A. The Behaviour of a Flexible Road Pavement under Accelerated Loading Test. *Bull. Transilv. Univ. Brasov. Eng. Sciences. Ser. I* **2018**, *11*, 257–266.
23. Cao, W.; Mohammad, L.; Barghabany, P. Use of indirect tension test and viscoelastic continuum damage theory for fatigue characterization of asphalt mixtures. *Constr. Build. Mater.* **2018**, *187*, 38–49. [\[CrossRef\]](#)

24. Luo, X.; Hu, S.; Zhou, F.; Crockford, W.; Karki, P. Simple Asphalt Mixture Shear Rutting Test and Mechanical Analysis. *J. Mater. Civ. Eng.* **2022**, *34*, 04022220. [[CrossRef](#)]
25. Ibrahim, O.; Yared, D.; Björn, B. Hierarchical approach for fatigue cracking performance evaluation in asphalt pavements. *Front. Struct. Civ. Eng.* **2017**, *11*, 257–269.
26. Mensching, D.; Daniel, J.; Underwood, B. Exploring indicators for fatigue cracking in hot mix asphalt pavements using simplified-viscoelastic continuum damage theory. *Road Mater. Pavement Des.* **2018**, *19*, 536–545. [[CrossRef](#)]
27. Fu, Y. Research on the Fatigue Damage of the Asphalt Pavement. *Appl. Mech. Mater.* **2012**, 256–259, 1776–1779.
28. Wu, Y.; Zhou, X.; Wang, X.; Shan, L. Long-Term Service Performance of Hard-Grade Asphalt Concrete Base Pavement Based on Accelerated Loading Test of Full-Scale Structure. *Sustainability* **2022**, *14*, 9712. [[CrossRef](#)]
29. Xu, X.; Yu, Y.; Yang, J.; Wu, C. Long-Term Skid Resistance Evaluation of GAC-16 Based on Accelerated Pavement Testing. *Adv. Mater. Sci. Eng.* **2020**, 2020, 1–9. [[CrossRef](#)]
30. Park, D. Evaluation of Predicted Pavement Fatigue Life Based on Surface Profiles and Asphalt Mixture Types. *KSCE J. Civ. Eng.* **2010**, *14*, 191–196. [[CrossRef](#)]
31. Xiao, Z.; Chen, M.; Wu, S.; Xie, J.; Kong, D.; Qiao, Z.; Niu, C. Moisture Susceptibility Evaluation of Asphalt Mixtures Containing Steel Slag Powder as Filler. *Materials* **2019**, *12*, 3211. [[CrossRef](#)] [[PubMed](#)]
32. Syyed, A.; Hunain, A.; Ahsan, W.; Muhammad, H.; Salman, H.; Junaid, M.; Abdullah, N.; Muhammad, A. Saving Energy in the Transportation Sector: An Analysis of Modified Bitumen Application Based on Marshall Test. *Energies* **2018**, *11*, 3025. [[CrossRef](#)]
33. Lv, S. Study on Low Temperature Performance Evaluation Index of Asphalt Mixture Based on Bending Test at Low Temperature. *Appl. Mech. Mater.* **2012**, 1931, 427–430. [[CrossRef](#)]
34. Li, Z.; Yu, W.; Ying, M. The Research of Low Temperature Performance of Asphalt Mixture. *Adv. Mater. Res.* **2010**, 168–170, 2507–2512.
35. Kim, M.; Mohammad, L.; Jordan, T.; Cooper, S. Fatigue performance of asphalt mixture containing recycled materials and warm-mix technologies under accelerated loading and four point bending beam test. *J. Clean. Prod.* **2018**, *192*, 656–664. [[CrossRef](#)]
36. *AASHTO TP 62*; Standard Method of Test for Determining Dynamic Modulus of Hot Mix Asphalt (HMA). American Association of State Highway and Transportation Officials: Washington, DC, USA, 2007.
37. *JTG E20-2011*; Standard Test Methods of Bitumen and Bituminous Mixtures for Highway Engineering. Ministry of Transport of the People's Republic of China: Beijing, China, 2011.
38. Nie, Y.; Zhang, Y.; Yu, J.; Kuang, D.; Zhang, X. Research on Aging Mechanism and Recycling Mechanism Based on Asphalt Four Components Analysis. *Appl. Mech. Mater.* **2012**, 1975, 1659–1664. [[CrossRef](#)]

Disclaimer/Publisher's Note: The statements, opinions and data contained in all publications are solely those of the individual author(s) and contributor(s) and not of MDPI and/or the editor(s). MDPI and/or the editor(s) disclaim responsibility for any injury to people or property resulting from any ideas, methods, instructions or products referred to in the content.